Summer 2016

Synthesis of Radioactive Nanostructures in a Research Nuclear Reactor

Maria Camila Garcia Toro

SYNTHESIS OF RADIOACTIVE NANOSTRUCTURES IN A

RESEARCH NUCLEAR REACTOR

by

MARIA CAMILA GARCIA TORO

A THESIS

Presented to the Faculty of the Graduate School of the

MISSOURI UNIVERSITY OF SCIENCE AND TECHNOLOGY

In Partial Fulfillment of the Requirements for the Degree

MASTER OF SCIENCE

in

NUCLEAR ENGINEERING

2016

Approved by

Carlos H. Castano Giraldo, Advisor
Joshua P. Schlegel
Joseph D. Smith

PUBLICATION THESIS OPTION

This thesis consists of the following papers prepared in the style utilized by the Journal of Applied Physics and Journal of Physical Chemistry Letters.

Paper I: Synthesis of Radioactive Gold Nanoparticles Using a Research Nuclear Reactor; pages 21-33, has been submitted for publication to the Journal of Applied Physics.

Paper II: Production of Bimetallic Gold – Silver Nanoparticles in a Research Nuclear Reactor; pages 49-73, will be submitted to the Journal of Physical Chemistry Letters.

The content of Section 5, Theoretical Estimation of The Total Absorbed Dose in MSTR; pages 34-48, will be published after experimental validation of the calculations.

ABSTRACT

In this work, the synthesis of radioactive nanostructures by water radiolysis was studied. The irradiation processes were done in the Missouri University of Science and Technology research nuclear reactor (MSTR).

Radioactive gold nanoparticles (AuNPs) were synthesized from aqueous solutions containing the metal salt precursors by radiolysis of water. Seven different samples were irradiated at 200kW of thermal power for 0.5, 1, 3, 5, 10, 30, and 60 minutes. The average sizes of the obtained nanoparticles ranged from 3 nm to 400 nm, it was found that the particle size decreased with the irradiation time. Some agglomerations of particles were found in each solution after the irradiation process. With this research, it was possible to synthesize, in a single step, radioactive AuNPs with the appropriate characteristics to be used in imaging diagnosis and cancer radiation therapy.

Radioactive bimetallic nanoparticles of silver and gold (Au/Ag BMNPs) were synthesized from aqueous solutions containing the metal salt precursors by radiolysis of water. Four samples with different Au/Ag concentration (30/70, 50/50, 70/30, and 0/100 by volume percentage) were irradiated at 10kW of thermal power for 3 minutes. The obtained nanoparticles showed (Au)core−shell(Ag) structure as well as alloyed metal structure depending on the solution concentration. It was found that the alloyed metal nanoparticles presented a faced centered cubic crystal structure with lattice parameter of 4.082 ± 0.001 Å and a chemical composition of 70.21 ± 0.01 wt% Au and 28.59 ± 0.01 wt% Ag.

ACKNOWLEDGMENTS

My completion of this Master degree could not have been accomplished without the support of my advisor Dr. Carlos H. Castano Giraldo; I must express my gratitude for his guidance, patience, and motivation to develop this research. I would also like to thank the members of the Committee Dr. Joshua P. Schlegel and Dr. Joseph D. Smith whom were involved in this work, I am thankful for their very valuable comments on this thesis and for their participation during my final defense. In addition, I really appreciate the support and help of Dr. Safwan Jaradat during the simulation process, and the support, help and friendship of my special friend, Lucy Sutcliffe, who has taught me valuable things during my learning time.

This thesis could not have been done without the funding opportunities from Nuclear Engineering Department of Missouri University of Science and Technology.

I would further like to thanks my parents, Flor and Jorge, for their dedication and support during all my life, my sister, Diana, for being the best sister and best friend for me, my friends in this city for accompanying me during this time.

Last, but not least, I want to express my very profound love and gratefulness to my boyfriend and best friend, Carlo, for providing me accompaniment, encouragement, understanding, and love during this time. His support enabled me to complete this process.

TABLE OF CONTENTS

LIST OF ILLUSTRATIONS

LIST OF TABLES

PAPER II

SECTION

1. INTRODUCTION

1.1. NANOTECHNOLOGY: IMPORTANCE AND APPLICATIONS

Nanotechnology refers to the science, engineering, and technology conducted at the nanoscale (10^{-9} m). One of the most important fields of nanotechnology is the development of nanomaterials. Nanomaterials include the creation of new materials and devices with unique chemical and physical properties arising from their dimensions [1].

The U.S National Nanotechnology initiative (NNI) [2] has defined a nanomaterial as any material smaller than 100nm and has described four generations of nanomaterials:

- Generation 1st: Passive nanomaterials (~2000). Materials that have passive participation in their applications, they act as chemical or physical agents to modify or enhance the properties of the medium where they are added. Some applications include coatings, filters, dispersions, ceramics, polymers, and others.

- Generation 2nd: Active nanomaterials (~2005). Materials that act as active agents in their applications. Some application examples include targeted and delivered drugs, transistors, sensors, molecular machines, nanoscale fluidics, and others.

- Generation 3rd: 3D Nanosystems and systems of nanosystems (~2010). Materials developed in three-dimensional structure with heterogeneous compositions to be applied in nanoscale components. Some applications include   structures and devices at the nanoscale with new architectures for biomedical   procedures.

- Generation 4th: Molecular Nanosystems (~2015). Materials with heterogeneous molecular nanosystems that are used as hybrid bioassemblies. Some applications

include molecules as devices, monitors and condition cells as nanobiosystems and multiscale self-assembled systems.

When a material is manufactured at nanoscale, its properties differ from the properties found in the bulk material. This phenomenon is known as quantum effects and they rule the behavior and properties of the nanomaterial. Therefore the nanomaterial properties are size-dependent and they can be tuned by controlling the particle size [1, 3].

Tunability of nanomaterial properties allows determining the appropriate characteristics to improve the material behavior for a specific application; hence it has given an extended range of applications for nanotechnology. Using nanotechnology, materials can effectively be made to be stronger, lighter, more durable, more reactive, more sieve-like, or better electrical conductors.

Applications of nanotechnology include energy, electronic, and chemical applications. Energy applications include solar cells, semiconductor nanostructures to be used in the next generation devices, cleaner and more affordable energy sources and consumer products to reduce energy consumption and toxicity to the environment.

Electronic applications include new computing, and communications devices to provide faster, smaller, and more portable systems that can manage and store larger amounts of information. Chemical applications include catalysts and inhibitors for chemical reactions, materials sintering processes, material characterization, transportation agents, storage agents, and others [1-3].

Nanotechnology has accomplished important contributions to medicine and biotechnology. Nanomedicine has improved the behavior of different methods and procedures to give more personalized, safer, cheaper, more portable, and easier solutions for the consumers. Some examples of advances in nanomedicine include [4]:

- Manufacture of semiconducting nanocrystals to enhance biological imaging for medical diagnosis. For example, quantum dots offer optical detection better than the conventional dyes used in biological tests (such as magnetic resonance imaging (MRI)) [5, 6].

- Development of an imaging technology to diagnose atherosclerosis. With the imaging analysis, the researchers are able to measure the amount of antibodies-nanoparticle complexes that accumulate specifically in plaques, in order to control the buildup of plaque in the arteries and the side effects of the treatments [7, 8].

- Development of a procedure to detection of early- stage Alzheimer's disease by using gold nanoparticles [9, 10].

- Production of nanostructures that spur the growth of nerve cells to treat damage in the spinal cord or in brain cells [11, 12].

- Application of multifunctional therapeutics nanostructures that serve as a platform to facilitate specific targeting to cancer cells and delivery of drugs minimizing risk to normal tissues [13].

1.2. NANOMATERIALS IN CANCER TREATMENT

According to the global status report on non-communicable diseases (NCDs) 2010 published by the World Health Organization (WHO) cancer and heart diseases are the principal causes of death around the world [14].

The American Cancer Society with the help of the National Cancer Institute, the National Program of Cancer Registries, the National Center for Health Statistics and the North American Association of Central Cancer Registries have projected that a total of 1,658,370 new cancer cases and 589,430 cancer deaths will have occurred in the United

States during 2015 [15]. It represents a challenge to improve the current cancer treatments in order to reduce the number of cancer deaths, therefor different research projects and billions of dollars are being invested to increase the knowledge about causes, treatments development, and new and more effective therapies that give the patients better possibilities to defeat the disease and extend life expectancy. Figure 1.1 shows the proportion of global deaths under the age of 70, by cause of death [14].
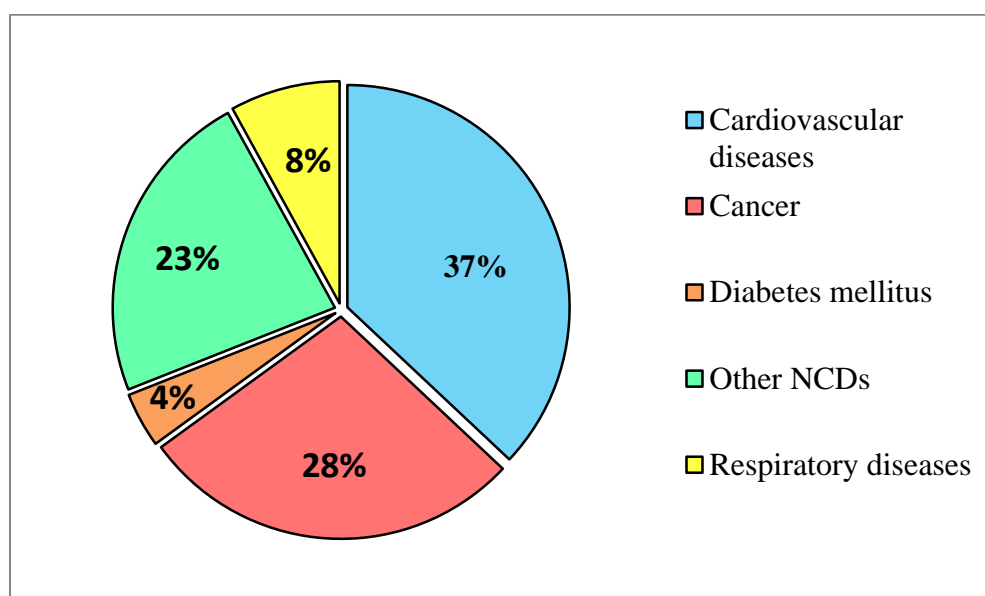
Figure 1.1. Proportion of global deaths under the age of 70 [14].

The application of nanomaterials in cancer treatment offers new prospects for the development of new non-invasive strategies for the diagnosis and treatment of cancer.

Nanomaterials can improve the performance of drug delivery, cancer cells' detention by imaging diagnosis, overcome biological barriers and enhance radiation

absorption [13]. The main benefit of nanotechnology in cancer treatment is the reduction of damage in normal tissue, radiation dose and side effects in patients by developing a strategy to increase the targeted radiation to the damaged cells. Some applications of nanotechnology for cancer treatment include:

1.2.1. Imaging Using Nanostructures. The medical imaging field has been leaded by x-ray, magnetic resonance imaging (MRI), and ultrasound (US) imaging. In the recent years, molecular imaging techniques have rapidly advanced to be potential imaging methods for clinical diagnosis in the future. The application of nanotechnology in medical imaging techniques improves the spatial resolution, sensitivity, signal penetration and multiplies the imaging targets and contrast agents [16]. According to the literature, it has been found that nanoparticles can be similar in size and share functionalities with cellular organelles (such as mitochondria, ribosomes, and transport vesicles) and these characteristics have been utilized to create unique imaging and therapeutic applications [17]. Some examples of imaging modalities using nanomaterials in their performances include: optical imaging (near-infrared (NIR) fluorescence imaging [17–20], Raman imaging [21]), US imaging (photoacoustic imaging [22]), MRI imaging [17, 23], X-ray/CT imaging [24, 25], multimodal imaging [26], and vascular imaging [27, 28].

Surface plasmon resonance (SPR) is a unique technique utilized for the detection and imaging of plasmonic materials [29]. Materials with this characteristic can absorb and scatter light regulated by the SPR characteristic frequency. Gold and silver nanoparticles are the most common and promising materials for this technique because their SPR phenomena are found in the visible to the near infrared region of the electromagnetic spectrum [30–33]. Furthermore, gold and silver nanostructures are

particularly interesting for biological applications because of their low reactivity, low toxicity profiles, and ease of functionalization [34–37]. Gold and silver nanoparticles have strong electric density and optical properties that make them interesting for thermal ablation applications, enhanced imaging agents, and contrast agents for electron microscopy. Some examples of gold nanostructures used in imaging diagnosis include spherical gold [38, 39], silica- gold nanoshells and gold nanorods [40, 41]. Alloyed gold/silver nanoparticles have been also studied for imaging diagnosis.

Other materials with excellent characteristics to be used in imaging diagnosis include superparamagnetic iron (SPIOs) nanoparticles that are useful for imaging contrast, separation, and generation of heat under alternating magnetic fields [13], carbon nanomaterials such as single-wall nanotubes, carbon dots, and graphene [42], nanoparticles based on gadolinium that are an excellent contrast agent [17, 23], and thorium dioxide nanoparticles as x-ray imaging contrast agent [24].

1.2.2. Nanoparticle-Mediate Radiosensitization. Nanomaterials have been used to make tumor cells more sensitive to radiation therapy by introducing them into the target cells. Radiation enhancers could cause more tissue damage by increasing the probability of ionization events leading to enhance the absorption or scattering of the radiation causing more local energy deposition and destroying tumor tissue.

Researches have demonstrated that the photoelectric mass attenuation coefficient is approximately proportional to the third power of the atomic number (Z) and materials with high-Z have greater photoelectric absorption producing considerable amounts of secondary electrons scattering from the surface of the high-Z material in the surrounding tissue [43, 44]. This process suppresses the growth of the tumor and produces necrosis in the tissue around metal implants after therapeutic irradiation [45–48]. Gold and silver

nanoparticles are excellent radiosensitizers due to their ability to increase the absorption of radiation energy and they can be preferentially targeted to the tumor tissue to spare normal tissue [34, 49, 50]. Other studies have also demonstrated that gold and silver radiosensitizer nanoparticles have enhanced the tumor dose in vitro and in vivo using x-ray sources, electron beams, and proton beams due to the more efficient interaction of lower energy radiation with high-Z materials through the photoelectric effect [51–55].

1.2.3. Radiation Protection with Nanoparticles. Looking at another side, some materials have been studied to improve the protection of normal tissue from radiation damage. Radiation induced injury to cell is caused by free radicals produced from the ionization events during the interaction of radiation with the tissue. These radicals have been the focus of extensive research to develop new methods for radiation protection.

This application is still under investigation because most of the materials used produce serious side effects in the patients include hypocalcemia, diarrhea, nausea, vomiting, sneezing, somnolence, hiccups, hypotension, and erythema multiforme [56]. Some nanomaterials used in radiation protection include cerium oxide [57], amifostine [56], and Carboxyfullerene [58, 59].

1.2.4. Brachytherapy. According with the Cancer Treatment Centers of America [60] brachytherapy is an advanced treatment for cancer diseases. This technique places radioactive sources in, on, or near the tumor giving a high radiation dose to the tumor tissue and at the same time reducing the radiation exposure in the surrounding healthy tissue. From the literature, it was found that the radiation dose produced by the radioactive source falls off with the distance quickly ($1/r^2$) giving low doses to the adjacent or distant normal tissue [61, 62].

There are different standard ways in which bracytherapy can be used to treat cancer [13]:

- Interstitial brachytherapy that consists of the insertion of radioactive sources directly into the tumor tissue. This implant is permanent until the required dose is delivered.

- Intracavitary brachytherapy that consist of the implant of a radioactive source into a cavity in the body. Devices used in this technique should be temporary.

- External applicators that are used when the tumor is close to the skin surface. The devices used in this technique are placed 0.5 to 1.0 cm away from skin surface.

It is important to note that nanoparticles of radioactive materials provide an opportunity to tune the radioactive therapeutic dose delivered to the tumor cells [63]. The most promising nanomaterial used in brachytherapy is radioactive gold nanoparticles because they have shown excellent properties [64–66].

Gold has two medically useful radioisotopes: ^{198}Au and ^{199}Au for cancer treatment. Their radionuclidic properties allow manipulating the nanoparticles during transportation and chemical process before clinical applications. Table 1.1 shows the radionuclidic properties of ^{198}Au and ^{199}Au.

^{198}Au is commonly produced by the neutron bombarding of natural gold (^{197}Au). Natural gold has high capture cross section for neutrons (100 barns) and the production of ^{198}Au isotope is efficient [13]. Colloidal gold has been used for interstitial irradiation in patients with prostatic cancer [67–69] and ovarian carcinoma treatment [70–72]. The colloidal is directly injected into the tumor or the nanoparticles can be functionalized using glucose, proteins, or polymer additives.

The principal advantage of using radioactive gold nanoparticles is the reduction of the chemotherapy time, dosage, and side effects. Some studies have demonstrated that

it is possible to kill cancer cells in tumors that have radioactive AuNPs using x-ray beam radiation instead of gamma rays [63, 66, 70].

Table 1.1. Radionuclidic properties of [198]Au and [199]Au isotopes.

Isotope	[198]Au	[199]Au
Half life	2.7 days	3.1 days
β average	312 keV	86 keV
β average	961 keV	453 keV
γ	412 keV	159 keV

1.3. MOTIVATION

Most of the published methods to synthesize radioactive gold nanoparticles and in general to produce radioactive nanomaterials include 2 different steps: the fabrication of nanoparticles and then activation by exposition to neutron source.

The synthesis of nanoparticles commonly includes chemical, physical, or biological processes [13, 34, 36, 38, 39, 71–77]. Only a few studies have reported methods to synthesize gold nanoparticles by using radiation with gamma sources [66, 78–84].Synthesis methods by two different steps can present some disadvantages such as expensive procedures, waste of time and loss of accuracy due to transition from one step to the next one.

The original contribution of this work is the development of an accurate method to synthesize radioactive nanostructures in a single step. The implementation of a research nuclear reactor to synthesize and activate radioactive nanostructure represents an innovation due to the presence of neutron radiation and ionizing radiation simultaneously. The methodology exposed in this work can represent advantages in cost, time, and accuracy of the production of radioactive nanostructures.

2. RESEARCH OBJECTIVES

2.1. GENERAL OBJECTIVE

The main objective of this work is the development of an effective method to synthesize, in a single step, radioactive nanostructures by using neutron radiation and ionizing radiation, controlling particle size, and chemical composition. A reduction process by radiolysis of water is the initiator of the synthesis of nanoparticles and the experiments are conducted in the research nuclear reactor of the Missouri University of Science and Technology.

2.2. SPECIFIC OBJECTIVE

Paper I

The objective of this paper is the production of radioactive gold nanoparticles by water radiolysis using a research nuclear reactor. The main goal in this study is to define the appropriate conditions to produce radioactive gold nanoparticles with specific characteristics to be used in cancer treatment.

Paper II

The objective of this paper is the production radioactive gold/silver bimetallic nanoparticles by water radiolysis using a research nuclear reactor. The leading target of this study is focused in the design of an accurate process to synthesize in a single step alloyed gold/silver nanoparticles with stable chemical composition and defined crystal structure.

3. RADIOLYSIS OF WATER

In radiation chemistry (the area involving the chemical effects induced by high-energy ionizing radiation), radiolysis of water is the decomposition of the molecules of water caused by ionizing radiation. The initial decomposition of water requires 13 eV and produces very reactive species such as $^\bullet H$, $^\bullet OH$, unstable ions, and electrons in aqueous solution that act as excellent oxidizing and reducing agents [85, 83].Water radiolysis has been the focus of many investigations due to its important role in different applications. It can be found during processes like food radiation, sterilization processes with radiation, sewage treatment, and radiotherapy [73, 86–88].The distribution of the products in the water decomposition is reflected by the linear energy transfer (LET) value that is the energy per unit path length deposited by the ionized particle in the medium. High LET radiation due to heavy ions, neutrons, and alpha particles can deposits energy densely whereas low-LET radiation due to high energy x-rays, accelerated electrons, and gamma radiation deposits the energy discretely along the path of the particle [89].

The reaction of water radiolysis can be defined as (equation 1):

$$H_2O \xrightarrow{ionizing\ radiation} e_{aq}^-,\ HO^\bullet, H^\bullet, HO_2^\bullet, H_3O^+, OH^-, H_2O, H_2 \qquad (1)$$
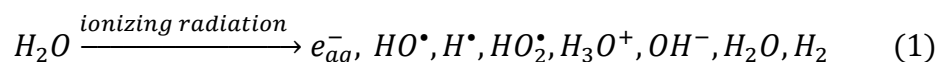
The reaction process occurs in three main stages: physical stage, physico-chemical stage, and chemical stage [89]. Figure 3.1 shows the main reactions that occur during the three stages of water radiolysis.

- The physical stage: occurs 1 fs (10^{-15} s) after the initial ionizing radiation process with the matter. It consists in the deposition of energy and the formation of ionized water

molecules (H_2O), exited water molecules ($H_2O^\bullet$) and sub-excitations electrons (e^-).

- The physico-chemical stage: occurs between 10^{-15} s and 10^{-12} s after the initial ionizing radiation process with the matter. In this stage several reactions occur including solvation of electrons, auto-ionization of excited states, ion-molecule reactions, and whole diffusion.

- The chemical stage: occurs between 10^{-12} s and 10^{-6} s. In this stage the species react with other molecules in the solute and then diffuse in the solution.
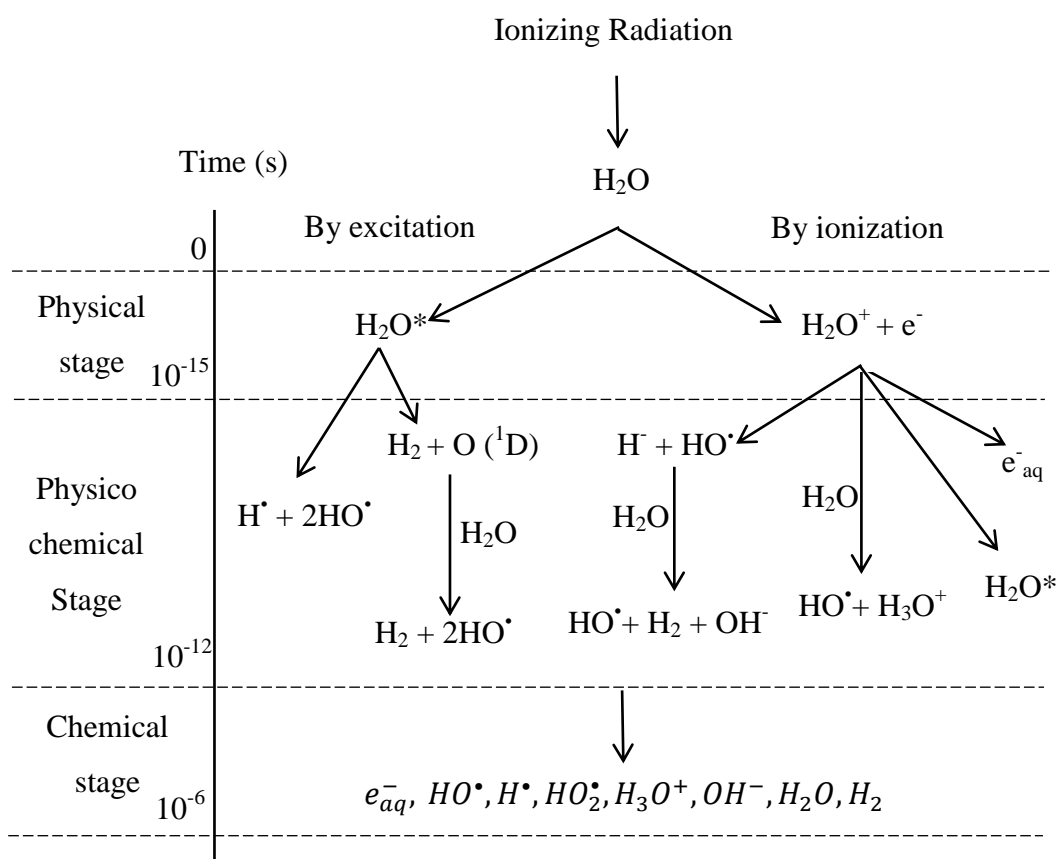
Figure 3.1. Mean reactions occurring during the three stages of water radiolysis.
Figure adapted from reference [89].

The species obtained from water radiolysis are very reactive. The hydroxyl radicals are very strong oxidative species with standard potential $E°$ ($HO^•/H_2O$) = 2.7 V_{NHE}. Hydrogen atoms and hydrated electrons are strong reducing agents with standard potentials $E^°$ ($H^+/H^•$) = -2.3 V_{NHE} and $E^°$ (H_2O/e_{aq}) = -2.9 V_{NHE} respectively.

When an aqueous metallic solution is irradiated, these free radicals can reduce dissolved metal ions (M^+) to their lower oxidation states until zero valence as shown in equation 2 and 3 [78, 79, 83, 89, 90]:

$$M^+ + e_{aq}^- \longrightarrow M^0 \tag{2}$$

$$M^+ + H^• \longrightarrow M^0 + H^+ \tag{3}$$

The metal atoms are formed with a homogeneous distribution throughout the irradiated solution due to the uniform energy deposition into the medium.

Since the binding energy between two metal atoms is stronger than the atom-solvent interaction energy, the atoms dimerize (equation 4) or associate with excess metal ions (equation 5) and finally metal clusters are formed by a multi-step coalescence process [78]. Figure 3.2 shows the metal nanoparticle formation under irradiation.

$$M^0 + M^0 \longrightarrow M_2 \tag{4}$$

$$M^0 + M^+ \longrightarrow M_2^+ \tag{5}$$
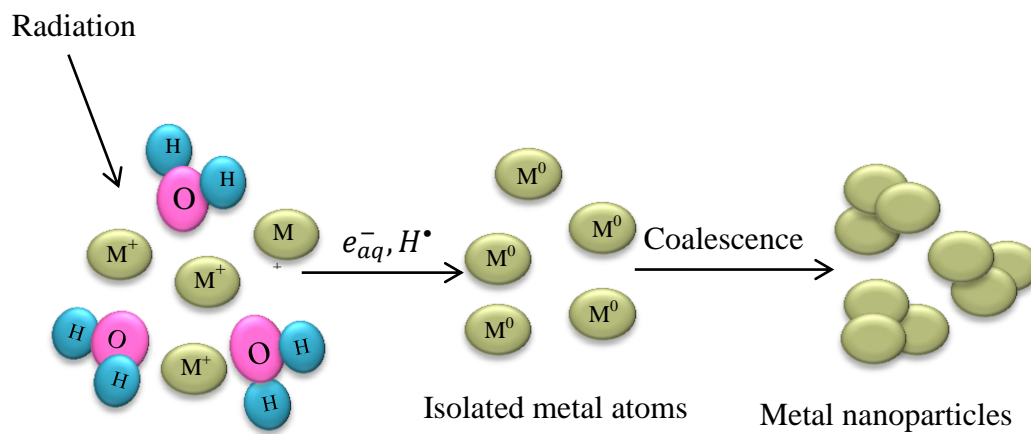
Figure 3.2. Metal nanoparticle formation under water radiolysis.

4. EXPERIMENTAL WORK

This section presents the experimental procedure to produce radioactive nanostructures by water radiolysis using a research nuclear reactor. The description includes the synthesis and characterization processes followed during the experiments. All experiments were conducted in the Missouri University of Science and Technology.

4.1. SYNTHESIS OF RADIOACTIVE NANOPARTICLES

The synthesis of radioactive nanoparticles was conducted in the research nuclear reactor of Missouri University of Science and Technology (MSTR). The procedure begins with the sample preparation by wet chemistry including the conditions for the radiation process.

4.1.1. Preparation of Solutions. The procedure to prepare the solutions for this work follows a previous reported method [81].

4.1.1.1. Radioactive gold nanoparticles - experiment. The chemical precursors for the solution that was used to produce gold nanoparticles were:

- Hydrogen tetrachloroaurate (III) trihydrate ($HAuCl_4.3H_2O$), ACS, 99.99% (metal basis), Au 49.5% min, purchased from Alfa-Aesar.

- Polyvinylpyrrolidone (PVP), 99.99%, as surfactant (colloidal stabilizer), purchased from Alfa-Aesar.

- 2–propanol HPLC, 99.7 +%, as the radical scavenger, purchased from Alfa-Aesar.

- Deionized (DI) water as a medium.

The $HAuCl_4.3H_2O$ was dissolved in DI water with dissolutions of 2-propanol and PVP to form primary solution with predetermined concentration of the metal salt of

2×10^{-3} M. PVP and 2-propanol were added with a volume ratio of PVP/2-propanol = 60, this ratio does not lead to any thermal reduction of the Au salt. The solution was mixed using a magnetic stirrer for 10 minutes to homogenize. Finally, the solution was bubbled with pure nitrogen for 30 minutes to remove oxygen.

4.1.1.2. Bimetallic gold/silver nanoparticles – experiment. The preparation of 2 mM solutions used to produce Au/Ag nanoparticles follows a similar procedure as the previous subsection. The chemical precursors for the solution that was used to produce Au/ Ag nanoparticles were:

- Hydrogen tetrachloroaurate (III) trihydrate ($HAuCl_4.3H_2O$), ACS, 99.99% (metal basis), Au 49.5% min, purchased from Alfa-Aesar.

- Silver nitrate ($AgNO_3$), ACS, 99.9% (metal basis), purchased from Alfa-Aesar.

- Polyvinylpyrrolidone (PVP), 99.99%, as surfactant (colloidal stabilizer), purchased from Alfa-Aesar.

- 2–propanol HPLC, 99.7 +%, as the radical scavenger, purchased from Alfa-Aesar.

- Deionized (DI) water as a medium.

Two solutions of 2 mM of $HAuCl_4.3H_2O$ and $AgNO_3$ were prepared using deionized water at room temperature. Dissolutions of PVP and 2-propanol were added to the solutions with a ratio by molar concentration of 1:60. These precursors acted as a colloidal stabilizer and a radical scavenger respectively. The mixture solution was bubbled up with Argon for 30 minutes to remove oxygen and avoid the reduction process due to secondary chemical reactions.

4.1.2. Radiation Process. The radiation process was conducted using the MSTR. The synthesis of radioactive gold nanoparticles was developed at 200 kW of reactor thermal power using different irradiation times. The synthesis of bimetallic Au/Ag

nanoparticles was developed at 10 kW of reactor thermal power with a irradiation time of 3 minutes each sample. Table 4.1 and 4.2 show the experimental conditions used in both experiments.

Table 4.1. Radiation process conditions to synthesize radioactive AuNPs in the MSTR at 200 kW of thermal power.

Experimental conditions	Sample 1	Sample 2	Sample 3	Sample 4	Sample 5	Sample 6	Sample 7
Time of irradiation (min)	0.5	1	3	5	10	30	60

Table 4.2. Radiation process conditions to synthesize Au/Ag BMNPs in the MSTR at 10 kW thermal power at 3 min/sample.

Experimental Conditions	Sample 1		Sample 2		Sample 3		Sample 4	
Chemical Composition (%)	Au	Ag	Au	Ag	Au	Ag	Au	Ag
	70	30	50	50	30	70	0	100

4.2. CHARACTERIZATION

The obtained nanoparticles were characterized by Transmission Electron Microscopy (TEM). During this microscopy technique, a beam of electrons is bombarded through the sample to form the image by the iteration of the electrons with the matter. This beam is guided by electromagnetic lenses that align the electrons into the beam allowing it to set the focus with accuracy.

Depending on the density of the material in the sample, some electrons are scattered from the beam when it hits the sample or they are able to pass through the material and hit a fluorescent screen producing a shadow image. The difference of densities produces varied darkness in the image and this characteristic allows the identification and classification of the samples analyzed.

In this work, the TEM was used to characterize the samples by imaging (to analyze the morphology and size distribution), energy dispersive spectroscopy (EDS - to identify the chemical composition of the samples), and selected area diffraction (SADP - to evaluate the crystal structure of the nanoparticles).

The TEM sample holders used to analyze the nanoparticles were Formvar/Carbon 300 mesh copper holders. The procedure to prepare the samples to the TEM analysis consisted in placing a small drop of the sample on the carbon surface of the grid. Then the samples were dried and placed in a grid holder to be transported to the electron microscopy lab.

The sample holders with the irradiated solutions were prepared three days after the irradiation process in order to allow the appropriate radiation decay of the samples before being inserted into the microscope. A strict method to manipulate the samples was followed as recommended by the Department of Environmental Health and Safety of

Missouri University of Science and Technology in order to keep the samples and the area as clean and safe as possible. Before taking the sample holders out of the reactor building, a Geiger Mueller detector was used to measure the radioactivity of the samples, and all of them presented doses in air lower than 0.003 mRad/hr at 2.54 cm.

PAPER

I. Synthesis of Radioactive Gold Nanoparticles Using a Research Nuclear Reactor

Maria C. Garcia Toro, Joshua P. Schlegel, Carlos H. Castano Giraldo

Department of Mining and Nuclear Engineering, Missouri University of

Science and Technology, 301 W. 14th St, Rolla, Missouri 65409 USA

Production of chemically stable, radioactive, gold nanoparticles in a single step is successfully accomplished using the Missouri S&T Research Nuclear Reactor (MSTR). A solution of gold chloride in a mixture of deionized water, polyvinylpyrrolidone (PVP), and 2-propanol is prepared. The volume ratio of PVP/2-propanol is 60. Seven different samples of the solution are irradiated at reactor thermal power of 200 kW for 0.5, 1, 3, 5, 10, 30, and 60 min. The obtained nanoparticles have a size distribution between 3nm and 450nm. It is found that the particle size depends on the time of irradiation; longer irradiation time produces smaller nanoparticles. Some agglomerated particles are found in all samples. The resulting nanoparticles are characterized with Transmission Electron Microscopy (TEM) and ImageJ.

I. INTRODUCTION

Cancer and heart diseases are the principal causes of death around the world.[1] The American Cancer Society, with the help of the National Cancer Institute, the National Program of Cancer Registries, the National Center for Health Statistics and the North American Association of Central Cancer Registries, have projected that a total of 1,658,370 new cancer cases and 589,430 cancer deaths will have occurred in the United

States during 2015.[2] Accordingly, billions of dollars are being invested in research to increase the knowledge about causes, biology, new drugs and development of newer and more effective therapies to reduce the death of cancer patients.

Some disadvantages in the current cancer therapies include the inability to bypass biological barriers, poor delivery and inadequate distribution of drugs inside the body, and difficult detection by imaging.[3] The application of nanotechnology in cancer treatment is helping overcome these limitations, giving the patients more possibilities to defeat the disease and extend life expectancy. Nanotechnology usage is the focus of exhaustive investigation in imaging and treatment.

Gold nanoparticles (AuNPs) have been shown good results in cancer diagnosis and treatment due to their high stability, low reactivity, low toxicity levels for the human body, and easy functionalization process.[4]–[6] AuNPs have been used to enhance imaging, photothermal therapy, chemotherapy, and radiation therapy by increasing the absorption or scattering of radiation.[7]–[10] The newest research in cancer treatment using gold nanoparticles includes ^{198}Au and ^{199}Au radioactive isotopes for locally irradiating and killing tumor cells. The properties of these isotopes (^{198}Au half-life = 2.7 days, β_{avg} = 312 keV, β_{max} = 961keV, and γ = 412 keV. ^{199}Au half-life = 3.1 days, β_{avg} = 86 keV, β_{max} = 453 keV, and γ = 159 keV) allow easy manipulation of the nanoparticles during transport and chemical processing before clinical applications.

The principal advantage of using radioactive AuNPs is the reduction of the chemotherapy time, dosage and side effects. Some studies have demonstrated that it is possible to kill cancer cells in tumors that have radioactive AuNPs using x-ray beam radiation instead of gamma irradiation.[11]–[13]

Many studies have been published about the different ways to produce radioactive AuNPs.[12]–[17] Most of them require two steps: first the nanoparticle are synthesized by chemical process and then activated with a neutron source. This work presents a novel method to produce radioactive AuNPs in a single step. The synthesis was done by radiolysis of aqueous solutions of gold chloride in the Missouri University of Science and Technology Nuclear Reactor (MSTR). The resulting nanoparticles where characterized with Transmission Electron Microscope (TEM) (Technai F20) and the Java-based image processing program ImageJ.

II. EXPERIMENTAL SECTION

For the experimental procedure, the chemical gold precursor was hydrogen tetrachloroaurate (III) trihydrate ($HAuCl_4.3H_2O$), ACS, 99.99% (metal basis), Au 49.5% min. The surfactant used (colloidal stabilizer) was polyvinylpyrrolidone (PVP), 99.99%. Both reagents were purchased from Alfa-Aesar. The radical scavenger was 2–propanol and the medium was purified and deionized water.

A solution of 2 mM of $HAuCl_4.3H_2O$ was prepared using deionized water at room temperature. Dissolutions of PVP and 2-propanol were added to the gold solution with a ratio of PVP/2-propanol = 60. This ratio does not lead to any thermal reduction of the Au salt. The mixture solution was bubbled with pure nitrogen for 30 minutes to remove oxygen. A similar procedure was demonstrated before. [18] The irradiation process was done in the MSTR operating at thermal power of 200kW. Seven different samples, of 2 ml each, were irradiated for 0.5, 1, 3, 5, 10, 30 and 60 minutes. The morphology of nanoparticles was characterized using TEM (Technai F20) and the size distribution was analyzed using ImageJ.

III. RESULTS

Production of chemically stable radioactive AuNPs in a single step from the irradiation of the precursor solution was successfully accomplished. The synthesis of nanoparticles is initiated by the radiolytic reduction of water by neutrons radiation and ionizing radiation. This reduction process creates solvated electrons (e_{aq}), H^+, OH^-, H_2O_2, and H_2 that are very reactive and reduced the metal ions present in the solution.[19]–[23] After the irradiation process, the solution changed color from light yellow to dark reddish. Samples that were irradiated for a short time presented lighter reddish color than samples that were irradiated for longer time. The difference in color change is due to the particle size obtained with different irradiation durations. Figure 1 shows TEM images of the seven samples, from shorter to longer irradiation time. The average particle size and their corresponding standard deviation (σ) are shown in Table 1.

TABLE I. Average particle size (nm) and variation with time of irradiation.

sample	irradiation time (min)	average size (nm)	σ (nm)
1	0.5	271	207
2	1	221	126
3	3	124	75
4	5	86	47
5	10	56	34
6	30	37	16
7	60	19	8
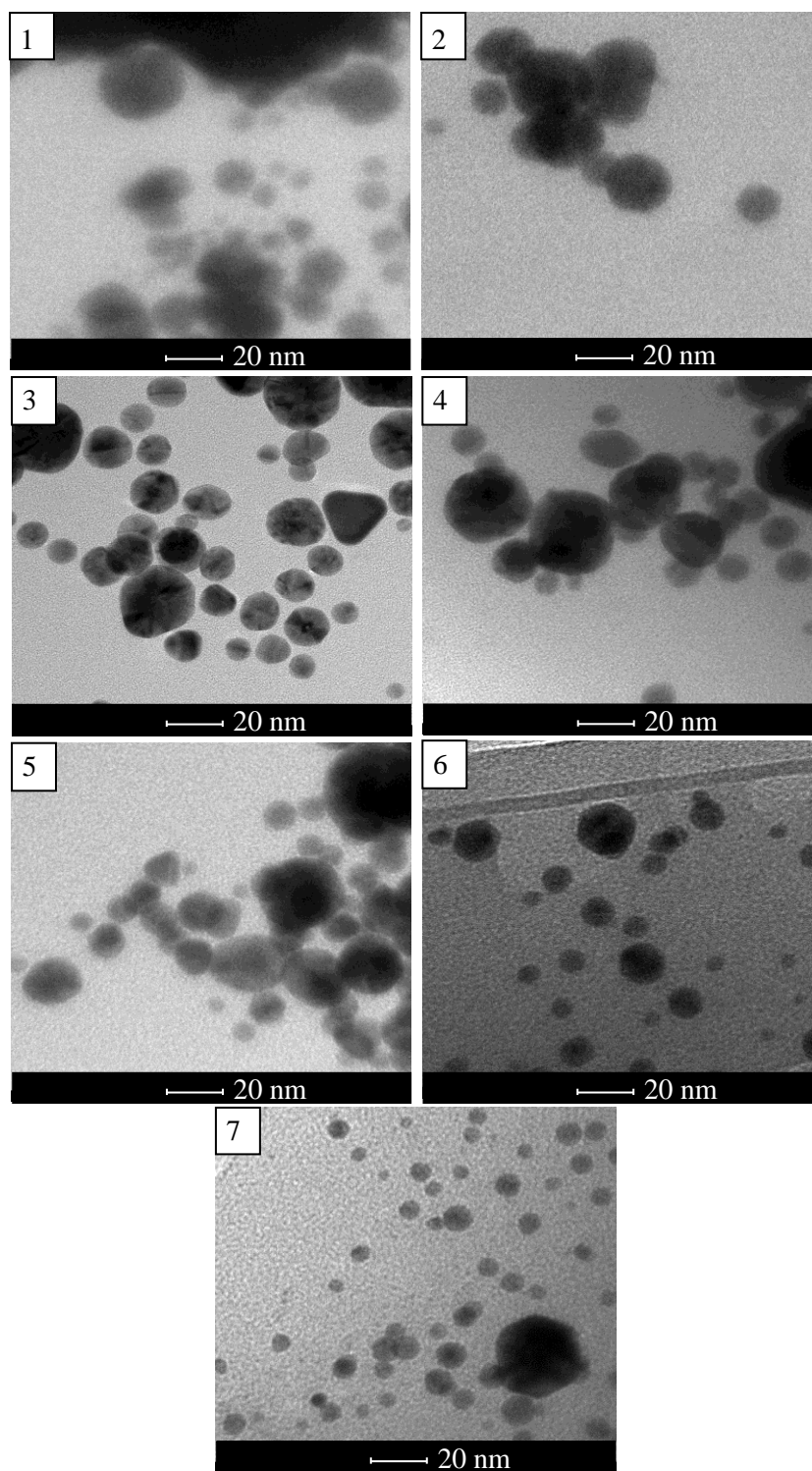
FIG. 1. TEM micrographs of the obtained radioactive gold nanoparticles that were irradiated at 200 kW for (1) 0.5 min, (2) 1 min, (3) 3 min, (4) 5 min, (5) 10 min, (6) 30 min, and (7) 60 min in the MSTR.

The TEM images show the presence of AuNPs in all samples, meaning that it is possible to synthesize NPs even with a short irradiation time. Despite of the addition of PVP to the solution, it was not possible to avoid the agglomeration of particles. However, most of the particles remained non-agglomerated. This agglomeration may be a consequence of the elapsed time between the irradiation process and the TEM analysis, since it was necessary to wait until the sample activity decayed enough to be safely transported and analyzed with the microscope in our current regulatory environment.

The variation of the average particle size and standard deviation with the irradiation time is shown in Figure 2. Both the particle size and standard deviation of AuNPs decrease with longer radiation times following a power trend with R-squared values of 0.968 and 0.996, respectively. After sixty minutes of irradiation a particle size reduction of 93% was achieved. However, most of the particle size reduction happened during the first ten minutes of irradiation (79%). After that time, the reduction rate lowered down to 3% every ten minutes. The same behavior was observed for the standard deviation.

According to previous research, the size distribution of AuNPs used in cancer treatment is a key element to improve tumor retention, interstitial interaction inside of the body, and the cancer cell killing process.[24]–[26] Those studies have demonstrated that particles with diameters between 1 nm and 100 nm are smaller than the size of the pores in the typical tumor vasculature allowing the AuNPs to access the cells in the tumor.[27]

However particles with diameters smaller than 10 nm can be removed from the body through the kidneys. Nanoparticles with approximately 50 nm of diameter exhibited greater sensitization and higher cell uptake compared with other sizes.[27]–[31] For this reason 50nm represents the most promising option for cancer treatment.

Accordingly, it is possible to obtain radioactive AuNPs with appropriate characteristics to be used in cancer treatment following the synthesis conditions used with sample 5 (10 min of irradiation time at thermal power of 200 kW).
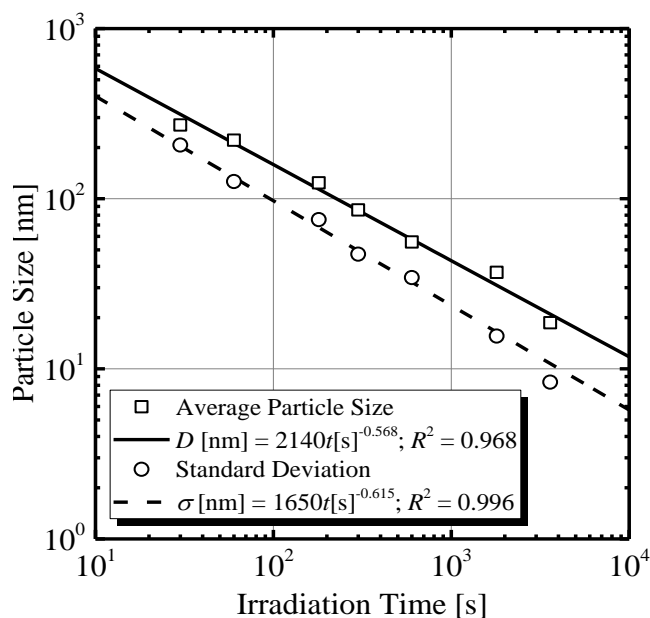
FIG. 2. Variation of average size and standard deviation with the irradiation time.

The average particle size is 56 nm with a standard deviation of 34 nm. Figure 3 shows the particle population vs. particle size for sample 5. Most of the obtained particles (95%) fall in the acceptable size range for cancer treatment (10 nm-100 nm) and almost half of them (32%) are the preferred particle size for cancer treatment (40 nm – 60 nm). The biggest particle size obtained in sample 5 was 296 nm; probably from particle agglomeration since it falls in an isolated size range. Chemical composition was verified

using Energy Dispersive Spectroscopy (EDS) in order to determine the possible presence of other chemical species. Figure 4 shows the EDS spectrum for sample 5 and Table 2 shows the composition in weight percentage and atomic percentage with the uncertainty for each element found in the spectrum.
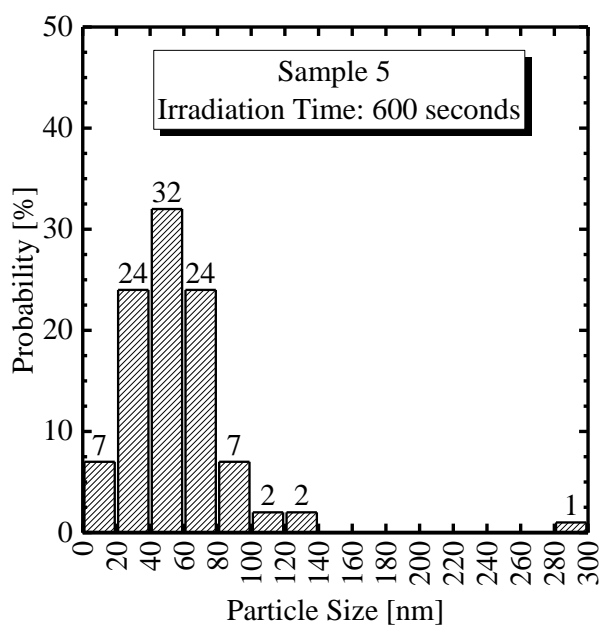
FIG. 3. Particle population vs particle size in nm for sample 5.

The TEM sample holders used were Formvar/Carbon 300 mesh copper holders, the medium used to prepare the sample was deionized water and the samples only contained gold chloride as a principal precursor. For that reason, the Cu, and C presence in the spectrum was ignored.

The weight percentage of gold in the sample demonstrates effective reduction of gold, producing metallic AuNPs without chemical contamination. The presence of Cl is

expected due to the precursor. The Cu and C presence in the spectrum is due to the

sample holder.

TABLE II. Composition in weight percentage and atomic percentage with
uncertainty for each element found in the spectrum.

element	weight %	atomic %	uncert. %
Cl (k)	28.3	68.7	3.0
Au (L)	71.7	31.3	9.9
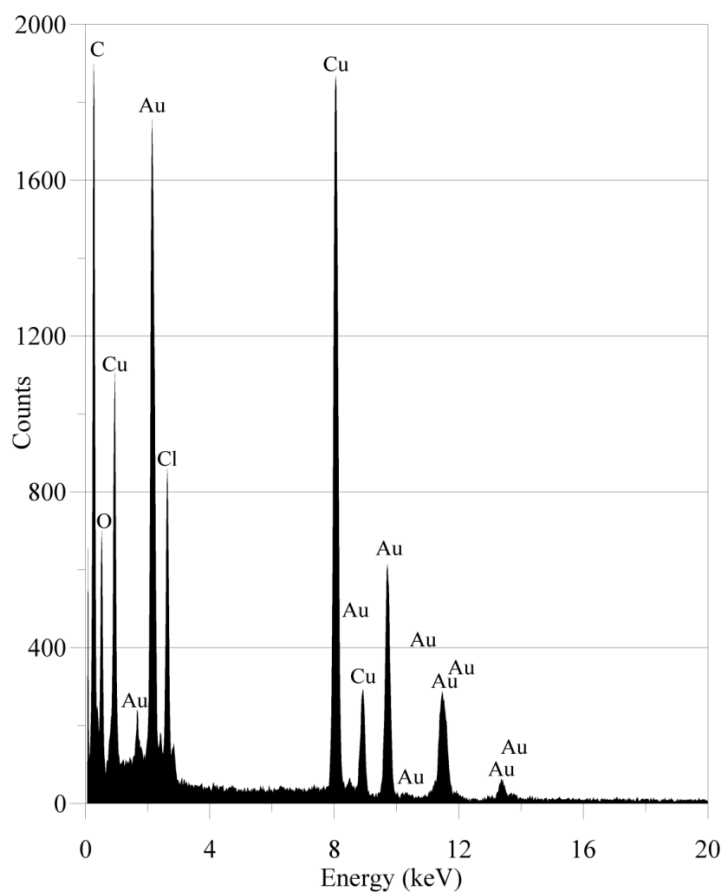
FIG. 4. EDS spectrum for sample 5.

IV. CONCLUSIONS

In conclusion, the synthesis in a single step of radioactive AuNPs by radiolysis was successfully accomplished following the described procedure. The gold nanoparticles produced presented good characteristics for use in cancer treatment. Future work will include in-vivo studies of these radioactive gold nanoparticles to identify their suitability and effectiveness.

V. ACKNOWLEDGEMENTS

VI. REFERENCES

[1]   World Health Organization, "Global status report on noncommunicable diseases 2010," *World Health*, p. 176, 2010.

[2]   R. Siegel, K. Miller, and A. Jemal, "Cancer statistics , 2015 .," *CA Cancer J Clin*, vol. 65, no. 1, p. 29, 2015.

[3]   J. Sajita, U. Gupta, and N. K. Jain, "Pharmaceutical and Biomedical Potential of Surface Engineered Dendrimers," *Crit. Rev. Ther. Drug Carrier Syst.*, vol. 24, no. 3, pp. 257–306, 2007.

[4]   T. S. Hauck, A. A. Ghazani, and W. C. W. Chan, "Assessing the Effect of Surface Chemistry on Gold Nanorod Uptake, Toxicity, and Gene Expression in Mammalian Cells," *Small*, vol. 4, no. 1, pp. 153–159, 2008.

[5]   E. E. Connor, J. Mwamuka, A. Gole, C. J. Murphy, and M. D. Wyatt, "Gold Nanoparticles are Taken Up by Human Cells but Do Not Causes Acute Cytotoxicity," *Small*, vol. 1, no. 3, pp. 325–327, 2005.

[6]   P. H. Davis, C. P. Morrisey, S. M. V Tuley, and C. I. Bingham, "Synthesis and Stabilization of Colloidal Gold Nanoparticle Suspensions For SERS," *Nanoparticles Synth. Stab. Passiv. Funct.*, vol. 996, no. 16, pp. 16–30, 2008.

[7]   J. Chen, D. Wang, J. Xi, L. Au, A. Siekkinen, A. Warsen, Z. Y. Li, H. Zhang, Y. Xia, and X. Li, "Immuno gold nanocages with tailored optical properties for targeted photothermal destruction of cancer cells," *Nano Lett.*, vol. 7, no. 5, pp. 1318–1322, 2007.

[8]   I. H. El-Sayed, X. Huang, and M. A. El-Sayed, "Selective laser photo-thermal therapy of epithelial carcinoma using anti-EGFR antibody conjugated gold nanoparticles," *Cancer Lett.*, vol. 239, no. 1, pp. 129–135, 2006.

[9]   A. M. Gobin, M. H. Lee, N. J. Halas, W. D. James, R. A. Drezek, and J. L. West, "Near-infrared resonant nanoshells for combined optical imaging and photothermal cancer therapy," *Nano Lett.*, vol. 7, no. 7, pp. 1929–1934, 2007.

[10]   M. P. Melancon, W. Lu, Z. Yang, R. Zhang, Z. Cheng, A. M. Elliot, J. Stafford, T. Olson, J. Z. Zhang, and C. Li, "In vitro and in vivo targeting of hollow gold nanoshells directed at epidermal growth factor receptor for photothermal ablation therapy," *Mol. Cancer Ther.*, vol. 7, no. 6, pp. 1730–1739, 2008.

[11]   M. Patyanik, A. Mayer, and I. Polgar, "Results of Ovary Tumor Treatment With Abdominally Administered 198Au Evaluated on the Basis of Long Term Follow Up," *Pathol. oncolgy Res.*, vol. 8, no. 1, pp. 54–57, 2002.

[12]   R. Kannan, V. Rahing, C. Cutler, R. Pandrapragada, K. K. Katti, V. Kattumuri, J. D. Robertson, S. J. Casteel, S. Jurisson, C. Smith, E. Boote, and K. V. Katti, "Nanocompatible chemistry toward fabrication of target-specific gold nanoparticles," *J. Am. Chem. Soc.*, vol. 128, no. 35, pp. 11342–11343, 2006.

[13]   R. Kannan, A. Zambre, N. Chanda, R. Kulkarni, R. Shukla, K. Katti, A. Upendran, C. Cutler, E. Boote, and K. V. Katti, "Functionalized radioactive gold nanoparticles in tumor therapy," *Wiley Interdiscip. Rev. Nanomedicine Nanobiotechnology*, vol. 4, no. 1, pp. 42–51, 2012.

[14]   J. Li, J. Wu, X. Zhang, Y. Liu, D. Zhou, H. Sun, H. Zhang, and B. Yang, "Controllable synthesis of stable urchin-like gold nanoparticles using hydroquinone to tune the reactivity of gold chloride," *J. Phys. Chem. C*, vol. 115, no. 9, pp. 3630–3637, 2011.

[15]   P. J. G. Goulet and R. B. Lennox, "New insights into Brust-Schiffrin metal nanoparticle synthesis," *J. Am. Chem. Soc.*, vol. 132, no. 28, pp. 9582–9584, 2010.

[16] S. K. Nune, N. Chanda, R. Shukla, K. Katti, R. R. Kulkarni, S. Thilakavathy, S. Mekapothula, R. Kannan, and K. V. Katti, "Green nanotechnology from tea: phytochemicals in tea as building blocks for production of biocompatible gold nanoparticles," *J. Mater. Chem.*, vol. 19, no. 19, p. 2912, 2009.

[17] V. Kattumuri, K. Katti, S. Bhaskaran, E. J. Boote, S. W. Casteel, G. M. Fent, D. J. Robertson, M. Chandrasekhar, R. Kannan, and K. V. Katti, "Gum arabic as a phytochemical construct for the stabilization of gold nanoparticles: In vivo pharmacokinetics and X-ray-contrast-imaging studies," *Small*, vol. 3, no. 2, pp. 333–341, 2007.

[18] T. Li, H. G. Park, and S. H. Choi, "gamma-Irradiation-induced preparation of Ag and Au nanoparticles and their characterizations," *Mater. Chem. Phys.*, vol. 105, no. 2–3, pp. 325–330, 2007.

[19] J. Belloni, M. Mostafavi, H. Remita, J.-L. Marignier, and M.-O. Delcourt, "Radiation-induced synthesis of mono- and multi-metallic clusters and nanocolloids," *New J. Chem.*, vol. 22, no. 11, pp. 1239–1255, 1998.

[20] J. V. Rojas and C. H. Castano, "Synthesis of rhenium oxide nanoparticles (RexOy) by gamma irradiation," *Radiat. Phys. Chem.*, vol. 99, pp. 1–5, 2014.

[21] J. V. Rojas and C. H. Castano, "Production of palladium nanoparticles supported on multiwalled carbon nanotubes by gamma irradiation," *Radiat. Phys. Chem.*, vol. 81, no. 1, pp. 16–21, 2012.

[22] J. V. Rojas and C. H. Castano, "Radiolytic synthesis of iridium nanoparticles onto carbon nanotubes," *J. Nanoparticle Res.*, vol. 16, no. 8, 2014.

[23] J. Rojas and C. H. Castano, "Production and Characterization of Supported Transition Metal Nano-Particles on Multi-Walled Carbon Nanotubes Functionalized By Gamma Irradiation and Chemical," in *Materials Processing and Energy Materials*, 2011, vol. 1, pp. 237–244.

[24] K. T. Butterworth, J. A. Coulter, S. Jain, J. Forker, S. J. Mcmahon, G. Schettino, F. J. Currell, and D. G. Hirst, "UKPMC Funders Group nm gold particles : potential application for cancer therapy," *Evaluation*, vol. 21, no. 29, 2011.

[25] D. M. Herold, I. J. Das, C. C. Stobbe, R. V Iyer, and J. D. Chapman, "Gold microspheres: a selective technique for producing biologically effective dose enhancement.," *Int. J. Radiat. Biol.*, vol. 76, no. 10, pp. 1357–1364, 2000.

[26] W. Chen and J. Zhang, "Using Nanoparticles to Enable Simultaneous Radiation and Photodynamic Therapies for Cancer Treatment," *J. Nanosci. Nanotechnol.*, vol. 6, pp. 1159–1166, 2006.

[27] S. Unezaki, K. Maruyama, J.-I. Hosoda, I. Nagae, Y. Koyanagi, M. Nakata, O. Ishida, M. Iwatsuru, and S. Tsuchiya, "Direct measurement of the extravasation of polyethyleneglycol-coated liposomes into solid tumor tissue by in vivo fluorescence microscopy," *Int. J. Pharm.*, vol. 144, no. 1, pp. 11–17, 1996.

[28] Arnida, A. Malugin, and H. Ghandehari, "Cellular uptake and toxicity of gold nanoparticles in prostate cancer cells: A comparative study of rods and spheres," *J. Appl. Toxicol.*, vol. 30, no. 3, pp. 212–217, 2010.

[29] Y. Aoyama, T. Kanamori, T. Nakai, T. Sasaki, S. Horiuchi, S. Sando, and T. Niidome, "Artifical viruses and their application to gene delivery. Sizecontrolled Nanoparticles., gene coating with glycocluster," *J. Am. Chem. Soc.*, vol. 125, pp. 3455–3457, 2003.

[30] B. D. Chithrani, A. A. Ghazani, and W. C. W. Chan, "Determining the size and shape dependence of gold nanoparticle uptake into mammalian cells," *Nano Lett.*, vol. 6, no. 4, pp. 662–668, 2006.

[31] T. Nakai, T. Kanamori, S. Sando, and Y. Aoyama, "Remarkably size-regulated cell invasion by artificial viruses. Saccharide-dependent self-aggregation of glycoviruses and its consequences in glycoviral gene delivery," *J. Am. Chem. Soc.*, vol. 125, no. 28, pp. 8465–8475, 2003.

[32] F. Osaki, T. Kanamori, S. Sando, T. Sera, and Y. Aoyama, "A quantum dot conjugated sugar ball and its cellular uptake. On the size effects of endocytosis in the subviral region," *J. Am. Chem. Soc.*, vol. 126, no. 21, pp. 6520–6521, 2004.

SECTION

5. THEORETICAL ESTIMATION OF THE TOTAL ABSORBED DOSE IN MSTR

In this section the total absorbed dose to produce radioactive gold nanoparticles is estimated. The process includes the method published by Martinho [91] and Monte Carlo N-Particle (MCNP) simulations to theoretically determine the total absorbed dose due to neutrons and gamma radiation when the reactor is operating. The content of this section will be published after validation of the calculations. The MSTR is a swimming pool-type research reactor that can reach 200 kW of thermal power and works with low-enriched Uranium (^{235}U) as fuel. The pool has 120 m^3 of high purity light water and the cooling system relies on natural convective flow. The reactor uses three control rods for coarse power control and emergency shutdowns, and a fourth control rod for fine power control. Figure 5.1 despicts the MSTR working at full power (200 kW) when it is possible to see Cherenkov radiation (blue glow). The current core configuration consists of 15 regular fuel elements that contain 18 fuel plates each, and 4 control rod fuel elements that contain only 10 fuel plates (the 8 middle fuel plates were removed to accommodate the control rods). The MSTR has low-enriched uranium silicide clad in aluminum as fuel, the plates are 0.152 cm thick and curved to allow for thermal expansion during operation [92]. Figure 5.2 presents a map of the current core configuration for MSTR. Each fuel element has a square section of 7.62 cm by 7.62 cm and a length of 91.44 cm with a cylindrical adapter at the bottom, which fits into the supporting grid plate [92]. The core is composed by fuel elements (F.E), control rod elements (C.R), a source tube, cadmium rabbit tube (C.R.T), hot cell tube (H.C) and bare rabbit tube (B.R.T).
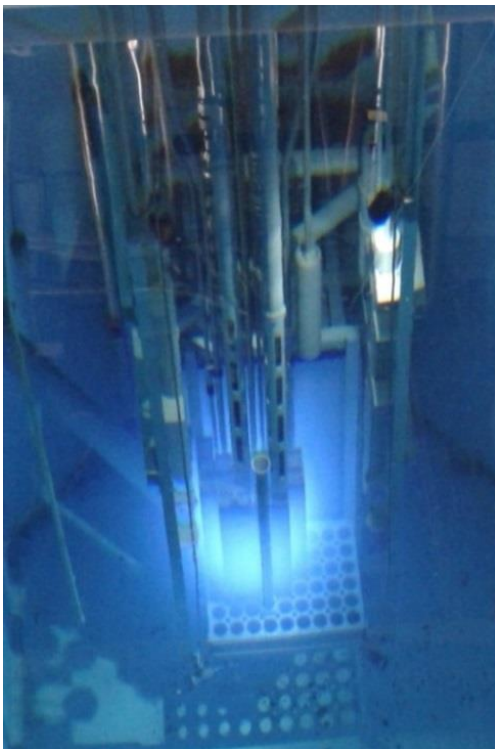
Figure 5.1. Picture of MSTR working at full power (200kW).

Figure 5.2. Core Configuration of MSTR.

5.1. ANALYTICAL CALCULATION

The absorbed dose is the energy absorbed per unit of mass of a system under irradiation due to the interaction between radiation and matter. The gray (Gy) is the unit of ionizing radiation dose in the International System of Units (SI) and it is defined as the absorption of one joule of radiation energy per one kilogram of matter (J/kg).

In the experiments conducted, the absorbed dose has two components due to neutrons and gamma radiation. The calculations were developed following the process described by Martinho, E. [91] and based in the following assumptions:

- The size of the samples and the boundary conditions allow fulfilling the charged particle equilibrium condition, making the kerma value equal to the absorbed dose.

- The absorbed dose due to neutrons is calculated using kerma factors and experimental neutron fluxes at the position where the samples were irradiated.

- The thermal, epithermal, and fast neutron flux are taken from previous experimental work described by Kulage, et al. [93].

- The absorbed dose due to gamma radiation is based on simulation results.

The total absorbed dose for the samples was calculated using equation 6:

$$D_{abs,total} = \dot{D}_t \times t_{irrad} \times Power\ of\ the\ reactor \qquad (6)$$

where $\dot{D}_t$ is the total dose rate, and t_{irrad} is the irradiation time. The total dose rate is the sum of the kerma rates due to the neutrons and the gamma dose rate as shown in equation 7:

$$\dot{D}_t = \dot{K}_n + \dot{D}_\gamma \qquad (7)$$

The total kerma rate was calculated adding the kerma rates of thermal (Th), epithermal (Epi) and fast neutron (fast) as described in equation 8:

$$\dot{K}_n = \dot{K}_{Th} + \dot{K}_{Epi} + \dot{K}_{fast} \tag{8}$$

The kerma rates were calculated using equation 9:

$$\dot{K}_n = \left(K_f \times \Phi\right)_{Th} + \left(K_f \times \Phi\right)_{Epi} + \left(K_f \times \Phi\right)_{fast} \tag{9}$$

where K_f is the kerma factor for a specific medium (in this case water), and Φ is the neutron flux.

The flux values for thermal, epithermal and fast neutrons at 200 kW of thermal power are shown in Table 5.1 [93].

Table 5.1. Flux values for thermal, epithermal and fast neutrons produced in the MSTR when the reactor is working at 200kW of thermal power [93].

Energy	Flux (neutrons/cm^{2}s)	Flux share of total
Thermal	2.94 x 10^{12} ± 1.9 x 10^{10}	38.99 %
Intermediate	1.86 x 10^{12} ± 3.7 x 10^{10}	24.62 %
Fast	2.65 x 10^{12} ± 3.0 x 10^{3}	35.15 %
Total	7.55 x 10^{12} ± 5.7 x 10^{10}	100.00 %

The kerma factor for water was calculated using the mean value of the kerma factor for each element [94] multiplied by the fraction of the total mass of the sample (w_i) corresponding to each element, as shown in equation 10:

$$K_f = \sum_i w_i \times (K_f)_i \qquad (10)$$

According to the National Institute of Standard and Technology (NIST) [95], the weight fraction in water is 11.19% for hydrogen and 88.81% for oxygen. Table 5.2 shows the kerma factors of oxygen, hydrogen, and water for each neutron energy.

The total kerma rate due to neutrons was calculated using equation 4 and the result is shown in Table 5.3. Based on the results shown in Table 5.3, the fast neutrons are the principal sources of kerma rate with 98.35% of participation.

Table 5.2. Kerma factors for oxygen, hydrogen and water for each neutron energy.

	Weight Fraction	K_f [Gy cm^2]		
		Thermal	Epithermal	Fast
Oxygen	0.89	3.50×10^{-19}	2.12×10^{-14}	2.61×10^{-12}
Hydrogen	0.11	4.20×10^{-14}	6.36×10^{-12}	2.54×10^{-10}
Water	1	4.70×10^{-15}	7.31×10^{-13}	3.07×10^{-11}

Table 5.3. Total kerma rate due to neutrons in Gy/s.

Energy	Thermal	Epithermal	Fast	Total
Kerma Rate (Gy/s)	0.01	1.36	81.47	82.84
Percentage	0.01 %	1.64%	98.35 %	100.00%

The total kerma rate was calculated using equation 4 considering the kerma rates for all neutron energies and the result is shown in equation 11:

$$\dot{K}_n = 82.84 \ \frac{Gy}{s} = 29.82 \ \frac{Mrad}{h} \qquad (11)$$

5.2. MCNP SIMULATION

Gamma dose rate was calculated using the MCNP code, which is a general-purpose code that can be used to calculate transport of neutron, photon, electron or combinations of them. The code treats an arbitrary three-dimensional configuration of materials in geometric cells bound by first and second degree surfaces and fourth degree elliptical tori [96].

Some areas of application of this code include radiation protection and dosimetry, radiation shielding, radiography, medical physics, nuclear criticality safety, detector design and analysis, nuclear oil well logging, fission and fusion reactor design, and others.

A complete model of the MSTR with accurate geometry, composition and components was made by Dr. Jeffrey King (Nuclear Science and Engineering, Colorado School of Mines, Golden, CO 80401, USA). This model was computed using MCNP version 5.1.51 with the nuclear data available in ENDF/B-VI.6 data library of the software [97]. A complete description of the MCNP code built for the MSTR is reported in previous publications [93], [97].

The model presents the whole reactor pool, the spent fuel storage pit, the portion of thermal column, and the beam port within the reactor pool. The reactor core includes all the fuel elements, rabbit tubes, control rods, and the grid plate on which the core rests. The support structure above the core was not included in the model.

Each fuel element is written as its own universe and placed using one of the transforms written for each grid space within the core. The fuel composition for each fuel element is based on the shipping documents received by the reactor during the conversion from highly enriched uranium fuel to the current low-enriched uranium fuel. The aluminum cladding and other aluminum pieces use compositions reported in the quality control reports. The concrete, stainless steel and borated stainless steel compositions are based on examples in the MCNP Primer [98], while the 1100-series aluminum compositions were found in MatWeb (1996-2011). Lead, cadmium, water, and graphite were defined to have naturally occurring isotopic compositions as reported in the chart of nuclides. A modified version of the MSTR code was used to simulate the gamma dose rate at the position of the sample vial (bare rabbit tube) when the reactor is working at full power. The code ran using track-length estimator tally (f4: n) and the tally multiplier card (fm4) with the reaction numbers -7, and -8 to obtain the number of neutrons produced per fission event (υ) and the energy produced per fission event (Q).

Also, the energy deposition tally (f6: p) and the tally multiplier card (fm6) were used to calculate the average of the absorbed dose due to gammas (Dγ) that are obtained per each started particle at the position of the sample vial. The code ran during approximately 4 hours using 40,304,812 particles histories. Table 5.4 shows the results obtained from the simulations.

Table 5.4. Results obtained with MCNP simulation.

υ	2.43	n / fission
Q	3.20×10^{-11}	J / fission
D_γ	2.17×10^{-15}	Gy / n

In order to know the total gamma dose rate produced in the irradiation process, it is necessary to know the number of neutrons per second produced in the irradiation process as shown in equation 12:

$$neutron\ rate = \frac{\upsilon \times power\ of\ the\ reactor}{Q} \tag{12}$$

Taking into account the results obtained from MCNP (Table 5.4) and the reactor thermal power, equation 12 is solved as followed:

$$neutron\ rate\ =\ \frac{2.43\ ^n/_{fission}\ \times\ 2.00\ x\ 10^5\ ^J/_s}{2.89\ x\ 10^{-11}\ ^J/_{fission}} \tag{13}$$

$$neutron\ rate\ =\ 1.68\ \times\ 10^{16}\ \frac{n}{s} \tag{14}$$

Therefore, the total gamma dose rate ($\dot{D}_\gamma$) produced in the irradiation process at the sample vial is the product of the gamma dose generated by each started particle and the neutron rate as shown in equation 15:

$$\dot{D}_\gamma\ =\ 2.17\ x\ 10^{-15}\ \frac{Gy}{n}\ \times\ 1.68\ x\ 10^{16}\ \frac{n}{s} \tag{15}$$

$$\dot{D}_\gamma\ =\ 36.41\ \frac{Gy}{s} = 13.10\ \frac{Mrad}{h} \tag{16}$$

Accordingly, the total dose rate was calculated using equation 2 and the results shown in equations 11 and 16:

$$\dot{D}_t\ =\ 82.84\ \frac{Gy}{s} +\ 36.41\ \frac{Gy}{s} \tag{17}$$

$$\dot{D}_t\ =\ 119.25\ \frac{Gy}{s}\ =\ 42.93\ \frac{Mrad}{h} \tag{18}$$

Finally, the total absorbed dose for the samples was calculated using equation 1 at 0.5, 1, 3, 5, 10, 30, and 60 minutes. During the final result calculation it is necessary to take into account the reactor power used to irradiate the samples and this value is used in equation 1 when the kerma rate and the gamma dose are calculated generically. However, in this study the reactor power was included during the calculation of kerma and gamma rates, and therefore the reactor power term was excluded from equation 1. Table 5.5 shows the estimated total absorbed dose to produce radioactive gold nanoparticles.

Table 5.5. Total absorbed dose to produce radioactive gold nanoparticles at 200kW.

Time of irradiation (s)	30	60	180	300	600	1800	3600
Total absorbed dose (Gy)	3577	7155	21465	35775	71550	214650	429300

In conclusion, considering the assumption described before in this section, the total absorbed dose rate is 119.25 Gy/s (42.93 Mrad/h) where the gamma dose rate contributes 30.53 % and the neutron kerma rate contributes 69.47% in the final result.

5.3. FURTHER RESEARCH

Future work will include the validation of the method presented in this section; the procedure will combine experimental results using the research nuclear reactor of the

Missouri University of Science and Technology with further simulations to verify the accuracy of the obtained data. Some preliminary data are shown below.

In order to prove the efficiency of the method used by Martinho [91] to calculate the neutron kerma rate, simulations in MCNP were done using the MSTR code to obtain the absorbed dose rate due to neutrons at the same position that the gamma dose rate was calculated. The energy deposition tally (f6: n) and the tally multiplier card (fm6) were used to calculate the average of the absorbed dose due to neutrons (Dn) that is obtained per each started particle. The code ran at the same conditions as the gamma dose simulations. The average of the absorbed dose due to neutrons generated per each started particle is:

$$D_n = 1.895 \times 10^{-15} \frac{Gy}{n} \tag{19}$$

Using the results shown in equation 19 and 14, it was possible to know the total neutron kerma rate produced in the irradiation process as shown in equation 20:

$$\dot{D}_n = 1.895 \times 10^{-15} \frac{Gy}{n} \times 1.68 \, x \, 10^{16} \frac{n}{s} \tag{20}$$

$$\dot{D}_\gamma = 31.836 \frac{Gy}{s} = 11.46 \frac{Mrad}{h} \tag{21}$$

Comparing the results for total kerma rate due to neutrons obtained with the method developed by Martinho [91] (82.84 Mrad/h) with the results for absorbed neutron

dose obtained with MCNP (11.46 Mrad/h), it was found that the two methods gave similar results, considering that they differ by less than one order of magnitude.

The difference is probably due to the assumptions that were taken into account during the calculations of Martinho's method. However, this result is not sufficient to prove the efficiency of Martinho's method, and it is necessary to verify if the obtained values from both methods are reasonable.In order to verify the veracity of the absorbed neutron dose results, it is necessary to corroborate first if the MCNP code can represent in a correct way the performance of the MSTR. An experimental work was done to obtain data that will be compared with MCNP results.

The experimental procedure consisted of an irradiation process to obtain an experimental value of gamma flux when the MSTR is working. This value will be used to be compared with the gamma flux obtained using the MCNP code at the same conditions that were set up during the experiments. The experiments consisted of two major parts; the first part consisted in finding the distance from the reactor core where only gamma radiation is found at 20W. Once the distance was defined, the power was gradually increased until it achieved full reactor power (200kW of thermal power) and more distances with only gamma radiation were found for each power level. At the final distance, the Geiger Mueller (GM) detector was placed to measure gamma flux.

The experimental setup includes a polyvinyl chloride (PVC) pipe was horizontally laid across the reactor pool and a 7.5 m long string attached to the PVC pipe was lowered until the pool bottom. A block of lead was attached as weight to the end of the string to keep straight the string. The sample was sealed in a vial and directly in line with the center of the core. Figure 5.3 shows the experimental setup to measure the gamma flux in the MSTR. Three different samples were used, one for each irradiation process. The

sample rotation was done in order to give the samples the necessary time to decay without affecting the continuity of the irradiation process.

The samples consisted of 42317 Silver foils, annealed, Premion, 99.998% (metals basis), 5 cm length, 1.5 cm width and 0.01cm thick. Table 5.6 shows the radioactive properties of ^{107}Ag and ^{108}Ag isotopes and Table 5.7 shows the samples weight in grams.
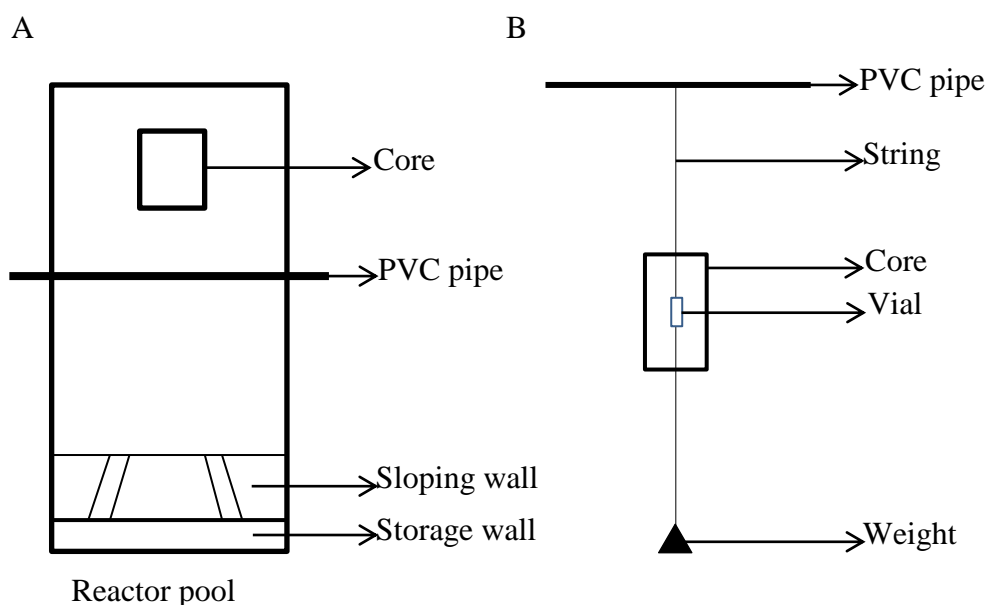
Figure 5.3. Experimental Setup to measure the gamma flux in the MSTR, top view of the PVP laid in the reactor pool (a), front view of the PVP laid in the reactor pool showing the position of the sample vial.

The results of the irradiation process are shown in Table 5.8. Six experiments were done at 20 W, 100 kW, and 200 kW to determine the distance from the reactor core where neutron activation is not found. When the reactor was working at full power, the

obtained distance from the reactor core where only gamma radiation is present was
1.321 m. The GM detector was located at this distance to measure gamma dose rate.

Table 5.6. Radioactive properties of Ag-107 and Ag-108 isotopes.

Nuclide Symbol	Isotopic mass	Half life	Decay mode	Daughter isotope
^{107}Ag	106.7	Stable		
^{108} Ag	107.9	2.37 min	β^- (97.15%)	^{108}Cd
			β^+ (2.85%)	^{108}Pd

Table 5.7. Weight in grams of the irradiated samples.

Sample 1	0.794 g ± 0.001g
Sample 2	0.814 g ± 0.001g
Sample 3	0.832 g ± 0.001g

Using the GM detector at 1.321 m from the reactor core, the gamma flux obtained
when the reactor is working at 200kW of thermal power was:

$$4.7 \, \frac{kRad}{h} = 47 \, \frac{Gy}{h} \tag{22}$$

The further work will be performed to modify the MCNP code creating a detector at 1.321 m far from the reactor code to run the code using f4:p and fm4 tallies in order to prove if the gamma dose rate obtained from the simulations is equal to the gamma dose rate obtained from the experimental work. If the results are similar it will be possible to affirm that the MCNP code can represent the correct behavior of the MSTR and the gamma dose rate obtained from MCNP at the position of the sample vial will be a correct value as well as the neutron dose rate calculated with the same code. Then, the described methodology will be able to verify the efficiency of the method developed by Martinho.

Table 5.8. Experimental results obtained from the irradiation process.

Sample	Power (kW)	Distance from the core (m)	Neutron activation (mrad/h)	Analysis
1	0.02	0.309 ± 0.003	0.60 ± 0.01	Activated
2	0.02	0.610 ± 0.003	0.03 ± 0.01	Non activated
3	100	0.610 ± 0.003	4.00 ± 0.01	Activated
1	100	1.219 ± 0.003	0.30 ± 0.01	Non activated
2	200	1.219 ± 0.003	1.00 ± 0.01	Activated
3	200	1.321 ± 0.003	0.40 ± 0.01	Non activated

PAPER

II. Production of Bimetallic Gold – Silver Nanoparticles in a Research Nuclear Reactor

Maria C. Garcia Toro, Joshua P. Schlegel, Carlos H. Castano Giraldo*

Department of Mining and Nuclear Engineering, Missouri University of Science and Technology, 301 W. 14th St, Rolla, MO 65409 USA

Corresponding Author

Email: castanoc@mst.edu

ABSTRACT

The synthesis of radioactive, bimetallic nanoparticles by water radiolysis was successfully developed using the Missouri S&T research nuclear reactor (MSTR). An aqueous solution of gold chloride and silver nitrate in a mixture of polyvinylpyrrolidone, and 2-propanol was prepared. The molar concentration ratio of PVP/2-propanol was 60. Four different samples with concentration ratio in percentage by volume Au to Ag of 70% / 30%, 50% / 50%, 30%/ 70%, and 100% of Ag were irradiated at a reactor thermal power of 10 kW for 3 minutes. The morphology, crystal structure, and chemical composition of the resulting nanoparticles where characterized with Transmission Electron Microscopy (TEM), Gatan Microscopy Suite Software and the Java-based image processing program ImageJ. The production of core-shell nanoparticles and alloyed nanoparticles was successfully accomplished and it was found that the obtained structure depends on the composition of the irradiated sample.

TOC GRAPHICS

KEYWORDS Bimetallic Nanoparticles, Radiolysis, Synthesis, Nuclear Reactor, MSTR

The development of nanostructures of multiple metals and alloyed metal represents a way to create new materials that show different structural, chemical, and physical properties that improve the behavior of the bulk material [1]. Bimetallic nanoparticles (BMNPs) have shown improved catalytic quality and performances due to their enhanced catalytic activity and selectivity in comparison with nanoparticles made using only one metal. These properties can be tuned modifying the size, composition, and structure of the nanoparticles [2–4]. Bimetallic nanoparticles have applications ranging from heat transfer, medicine, chemical processes, electrochemical processes, electronic technology, aerospatial industry, and others [1, 2, 5–7].

Different methods to synthesize BMNPs are available including chemical processes (such as sol-gel, impregnation method, liquid reduction method, and others), biological processes, physical processes, and radiochemical reduction processes [2, 5, 8, 9].

This work shows the production of radioactive BMNPs by radiolysis of water, in a single step, using a research nuclear reactor.

Water radiolysis can be represented by equation 1:

$$H_2O \xrightarrow{ionizing\ radiation} e_{aq}^-,\ HO^\bullet, H^\bullet, HO_2^\bullet, H_3O^+, OH^-, H_2O, H_2 \qquad (1)$$
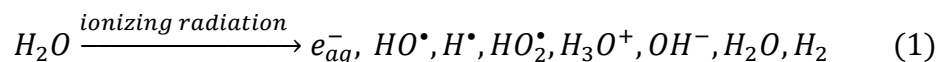
The species obtained from water radiolysis are highly reactive and can reduce metal ions. When a solution of metallic ions is irradiated, the reduction of metallic ions is reached until zero valence as shown in equations 2 and 3 [10–13, 8]:

$$M^+ + e_{aq}^- \longrightarrow M^0 \qquad (2)$$

$$M^+ + H^\bullet \longrightarrow M^0 + H^+ \qquad (3)$$

After the reduction process, the atoms dimerize or associate with other ions forming metal clusters that produce metallic nanostructures by coalescence processes. The bimetallic nanoparticles can be obtained as an alloy of the metals or as a core-shell structure. The production of core-shell clusters by radiolysis depends on the electro chemical characteristics of the metals ions in solution. When a metallic ion (M_a^+) is in a solution with other metallic ion (M_b^+) both of them have the same probabilities to be reduced by radiolytic radicals produced in water radiolysis. However, the less noble metallic ion acts as an electron donor to the nobler metallic ion and a further electron transfer between them occurs favoring first the reduction of the nobler metal [8].

Assuming M_a^+ as the nobler metallic ion and M_b^+ as the less noble metallic ion, equation 4 shows the reaction of the reduction of the nobler metallic ion by electron transfer from the less noble atom:

$$M_a^+ + M_b^0 \longrightarrow (M_a M_b)^+ \longrightarrow M_a^0 + M_b^+ \qquad (4)$$
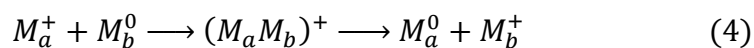
When the metallic ion is plurivalent the probability of segregation increases with the electron transfer between the intermediate–low valences of both metals. The nobler metallic ions receive electrons from the less noble metallic ions and monometallic clusters M_a are obtained first. Then, when the M_a^+ ions are spent, the M_b^+ ions are reduced thereafter on the surface of M_a. The final result is the production of a core–shell cluster where the nobler metal is coated by the lesser one.

The production of alloyed clusters occurs when the intermetal electron transfer is not obtained even during long irradiation times [14]. The metal ions are reduced by the radicals obtained from water radiolysis (equation 1). This process produces atoms of both metals and it is followed by mixed coalescence. Equations 5 and 6 represent the coalescence process of the metallic atoms:

$$M_a + M_b \longrightarrow (M_a M_b) \qquad (5)$$

$$(M_a M_b) + M_a \longrightarrow (M_{a,2} M_b) \qquad (6)$$
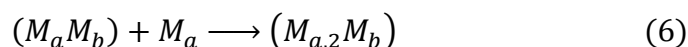
The union of atoms and clusters with ions is also possible during the reduction process and the reaction is represented in equation 7:

$$(M_a M_b)^+ \ + M_a{}^+ \longrightarrow (M_{a,2} M_b)^{2+} \tag{7}$$
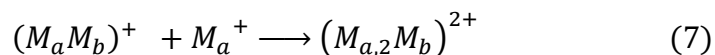
These associations allow the production of bimetallic alloyed clusters according to the relative initial ion concentration [8].

The formation of an alloyed or a core-shell cluster depends on the kinetic competition of the electron transfer from the less noble to the nobler metal ions (equation 4) and on the radiation-induced reduction of both metal ions (equation 7). This competition depends on the chemical characteristics of the metal and also on the dose rate.

 A powerful and sudden irradiation process could prevent the electron transfer between both metal ions, and the metallic atoms are produced fast and with total reduction [8]. Then, the coalescence of those atoms forms alloyed clusters. In other words, a high dose rate of ionizing radiation may kinetically favor alloyed metal nanoparticles rather than the normally formation of core-shell nanoparticles, which are favored if the formation reactions occur under thermodynamically controlled conditions [15]. Figure 1 shows the difference between core-shell clusters production and alloyed clusters production.
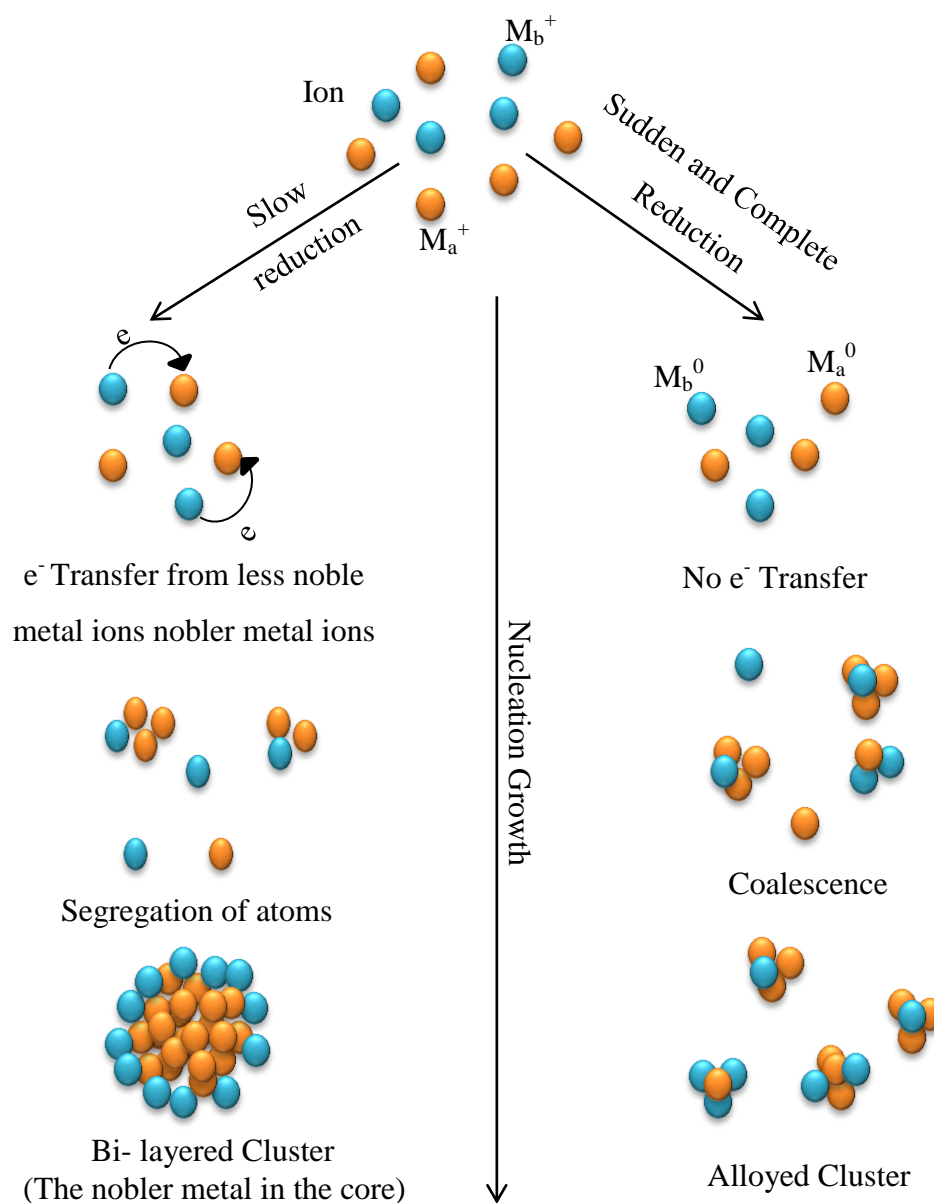
Figure 1. Difference between core-shell clusters production and alloyed cluster production. Figure adapted from reference [8].

In this work, radioactive gold/silver BMNPs are produced by radiolysis of water, using the MSTR. AuAg-BMNPs have good optical properties that depend on the composition, geometrical structure, and capability of adsorbing near infrared irradiation. Their

applications include biomedical recognition processes, biosensing, drug delivery, photothermal therapy, and molecular imaging [2], [16].

The chemical gold precursor used is hydrogen tetrachloroaurate (III) trihydrate ($HAuCl_4.3H_2O$), ACS, 99.99% (metal basis), Au 49.5% min, the chemical silver precursor is silver nitrate ($AgNO_3$), ACS, 99.9% (metal basis), and the surfactant used (colloidal stabilizer) was polyvinylpyrrolidone (PVP), 99.99%. These reagents were purchased from Alfa-Aesar. The radical scavenger was 2–propanol and the medium was purified and deionized water.

Two solutions of 2 mM of $HAuCl_4.3H_2O$ and $AgNO_3$ were prepared using deionized water at room temperature. Dissolutions of PVP and 2-propanol were added to the solutions with a ratio by molar concentration of 1:60, this ratio does not lead to any thermal reduction of the metallic salts [17]. The mixture solution was bubbled up with Argon for 30 minutes to remove oxygen. The deaeration process is important to prevent oxidation reactions caused by dissolved oxygen before and during the irradiation process, allowing the oxidation–reduction process exclusively from water radiolysis [15]. A similar procedure was demonstrated before [18].

The irradiation process was conducted in the MSTR operating at 10kW of thermal power. Four different samples of 2 ml were irradiated for 3minutes. The compositions of the samples are shown in Table 1. The morphology, chemical composition and crystal structure of the nanoparticles were characterized using Transmission Electron Microscopy (TEM-Technai F20), Gatan Microscopy Suite Software, and ImageJ.

Table 1. Composition in volume percentage of the four samples irradiated in the MSTR.

Sample	Composition (vol %)	
	HAuCl4.3H2O	AgNO3
1	70	30
2	50	50
3	30	70
4	0	100

The production of Au/Ag BMNPs was successfully accomplished. The synthesis of nanoparticles was initiated by the reduction process due to the products obtained from water radiolysis [10], [12], [13]. The irradiated Au/Ag solutions presented a color change from light yellow to light reddish. This is caused by the reduction of the metallic salts and depends on the concentration of $AgNO_3$ and $HAuCl_4.3H_2O$ in solution; as the Au/Ag molar ratio increased, the intensity of the reddish color increased. According to previous work, the silver nitrate plays a special role on the behavior of gold atoms during growth, the silver assisted growth is slower and gold atoms grow a structure with no defect [19]. The morphology, crystal structure, and chemical composition analyses of the Au/Ag BMNPs show that both core-shell and alloyed metal structures were obtained. Figure 2 shows the TEM images of the four samples irradiated in the MSTR.

The TEM micrographs show that particles from sample 1 (Figure 2.a) presented a multi-spiked structure formed due to coating of metal nanoparticles. Particles from sample 2 (Figure 2.b) presented a homogeneous deposition of metal nanoparticles on the surface.

Samples 3 (Figure 2.c) and 4 (Figure 2.d) presented nanoparticles with uniform surface without the deposition of nanoparticles. The results above are consistent with previous studies [1, 5, 7, 9, 16], demonstrating that samples 1 and 2 presented nanoparticles with core-shell structure while sample 3 presented nanoparticles with alloyed metal structure.
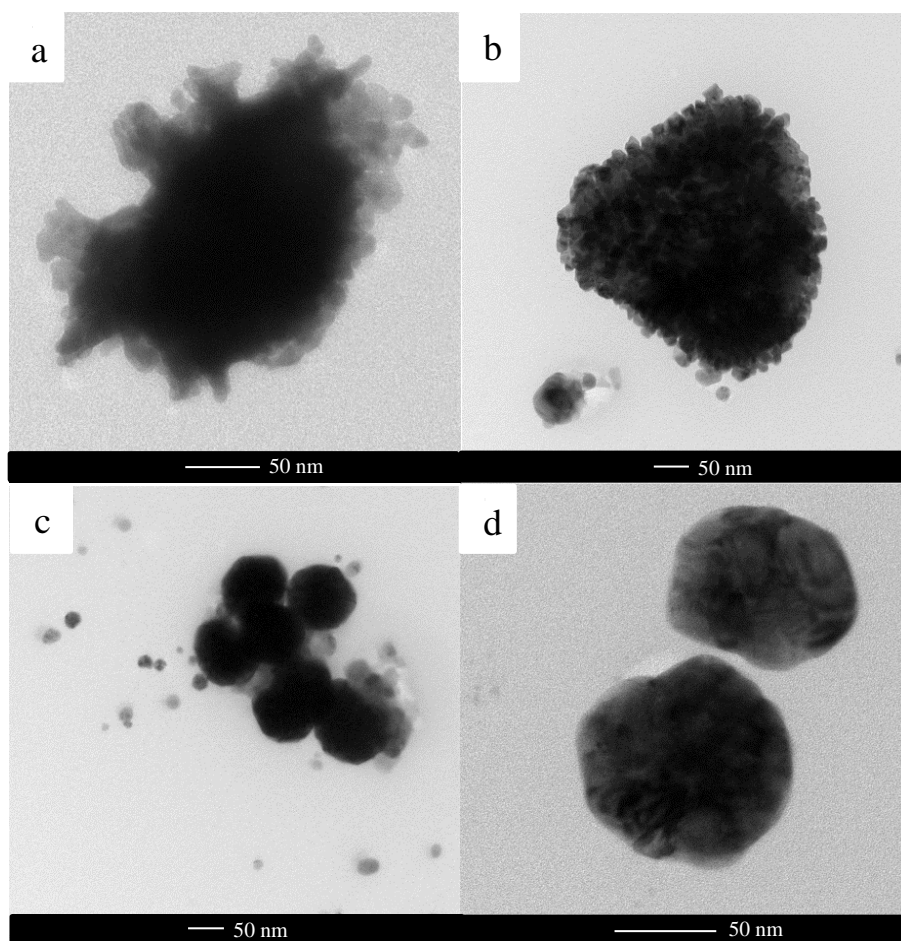
Figure 2. TEM micrographs of Au/Ag BMNPs obtained from the irradiation of the four different samples in the MSTR.

Nanoparticles from sample 4 are composed of pure Ag without the presence of other chemical components due to the composition of the irradiated sample.

In order to confirm the bimetallic composition, the energy dispersive spectroscopy (EDS) and selected area diffraction patterns (SADPs) analysis were conducted to evaluate the chemical composition of the nanoparticles and their crystalline structure. The EDS of sample 1, 2 and 3 showed the presence of Au and Ag in each nanoparticle composition, proving that the production of BMNPs was achieved. However, the presence of Cl was also detected in all samples; it could mean that the formation of AgCl occurred due to the chemical reaction between $AgNO_3$ and the Cl⁻ from the gold precursor. Therefore, the composition of the bimetallic nanoparticles could include some Au/AgCl. As mentioned before, sample 4 presented only Ag in the nanoparticles composition because of the composition of the irradiated sample.

EDS spectra for the four analyzed samples is presented in Figure 3. The composition in weight percentage, atomic percentage and uncertainty for each element found in the spectra is presented in Table 2. The presence of copper and carbon in the spectra is due to the composition of the TEM sample holders (Formvar/Carbon 300 mesh).

The SADPs of the Au/Ag BMNPs from the four samples were analyzed comparing them to the SADPs of the pure metals (Au and Ag) and AgCl in order to verify the crystal structure and the presence of alloyed metal nanoparticles.
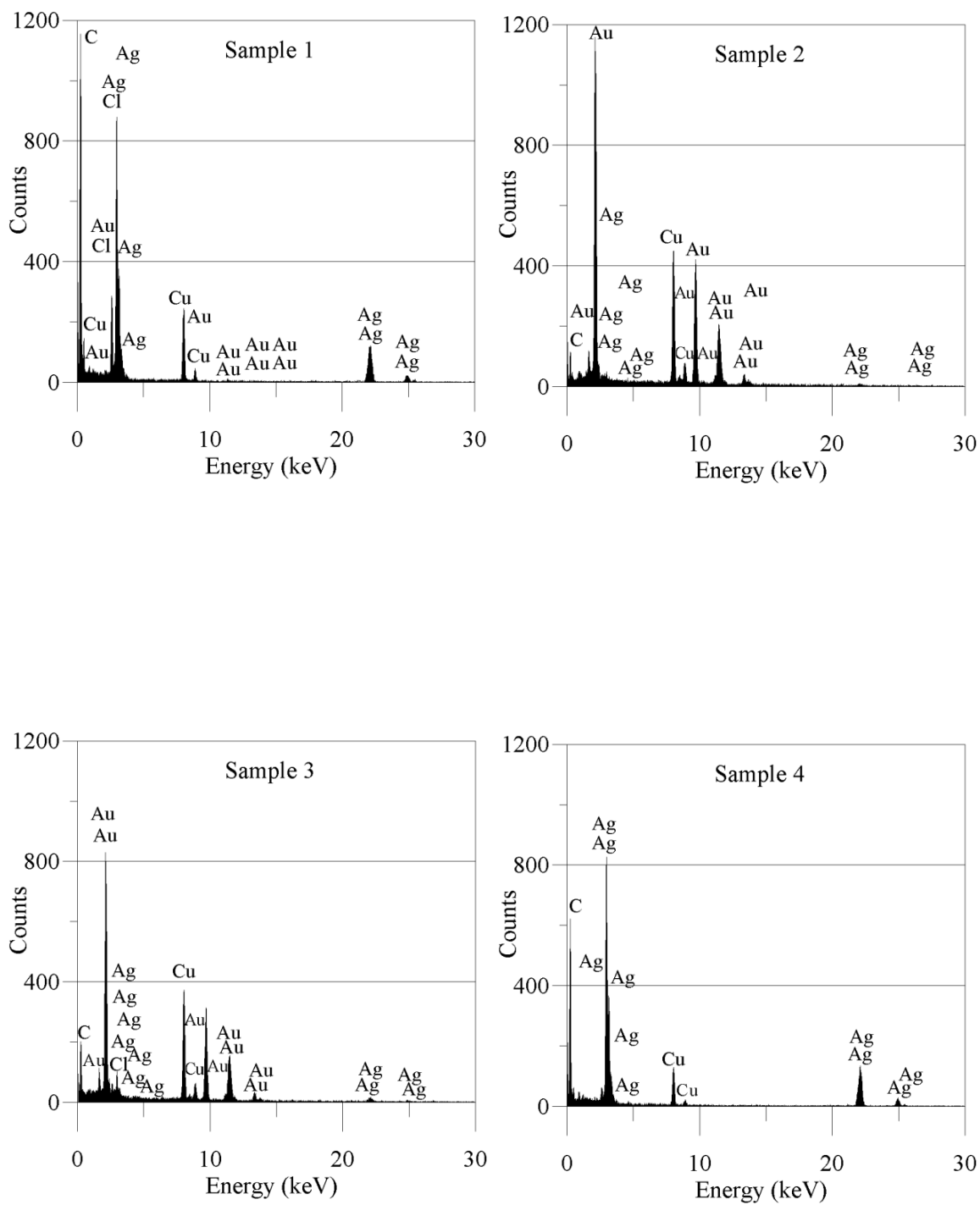
Figure 3. EDS spectra of Au/Ag nanoparticles of the four irradiated samples.

Table 2. Composition in weight percentage, atomic percentage and uncertainty percentage for each element found in the EDS spectra.

Sample 1				Sample 2			
Element	Weight % (± 0.01)	Atomic % (± 0.01)	Uncert. % (± 0.01)	Element	Weight % (± 0.01)	Atomic % (± 0.01)	Uncert. % (± 0.01)
Au	10.88	10.41	0.19	Au	87.55	85.30	1.25
Ag	78.89	63.76	1.62	Ag	12.34	14.18	0.20
Cl	10.23	25.83	0.28	Cl	0.11	0.52	0.02
Sample 3				Sample 4			
Element	Weight % (± 0.01)	Atomic % (± 0.01)	Uncert. % (± 0.01)	Element	Weight % (± 0.01)	Atomic % (± 0.01)	Uncert. % (± 0.01)
Au	70.21	61.74	1.32	Au	0.00	0.00	100.00
Ag	28.59	32.27	0.49	Ag	100.00	100.00	1.59
Cl	1.20	5.99	0.09	Cl	0.00	0.00	0.11

Simulations of the Au, Ag, AgCl, and Au/Ag patterns were run using Web Electron Microscopy Applications Software (WebEMAPS) of the Department of Materials Science and Engineering, University of Illinois at Urbana-Champaign [20].

The d-spaces for each pattern were obtained from the simulations (see appendix). Figure 4 shows the SADPs for pure gold (4.a) and pure silver (4.b). Table 3 shows the characteristics of the crystal structures of pure Au, pure Ag and AgCl.
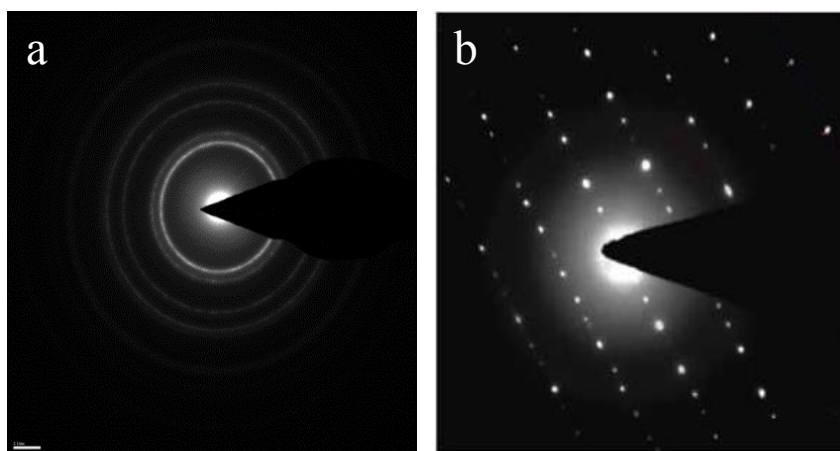
Figure 4. Selected area diffraction pattern for pure gold (a) and pure silver (b).

Table 3. Characteristics of the crystal structures of pure Au, pure Ag and AgCl.

	Au	Ag	AgCl
Atomic Radius	174 pm	165 pm	_
Crystal Structure	Face centered cubic	Face centered cubic	Face centered cubic
Lattice angles	$\pi/2, \pi/2, \pi/2,$	$\pi/2, \pi/2, \pi/2,$	$\pi/2, \pi/2, \pi/2,$
Lattice parameters [Å]	4.078	4.085	5.549
Space group name	Fm_3m	Fm_3m	Fm_3m
Space group number	225	225	225

From Table 3, the crystal structures of the BMNPs are expected to be face centered cubic (fcc). According to the information presented in the introduction; the core-shell nanoparticles would present the SADP for pure silver (or AgCl) because the core is composed by Au atoms. The alloyed metal nanoparticles would present a crystal structure

with lattice parameter between the values obtained for pure Au and pure Ag (or AgCl). Sample 1, 2 and 4 presented similar SADP. Analyzing their patterns, it was found that the d-spaces obtained belong to the pure Ag with a lattice parameter of 4.087 ± 0.001Å, that means that the nanoparticles obtained from sample 4 are pure Ag as are the shell structures of the nanoparticles obtained from sample 1 and 2. . The SADP obtained for sample 1 is shown in Figure 5.
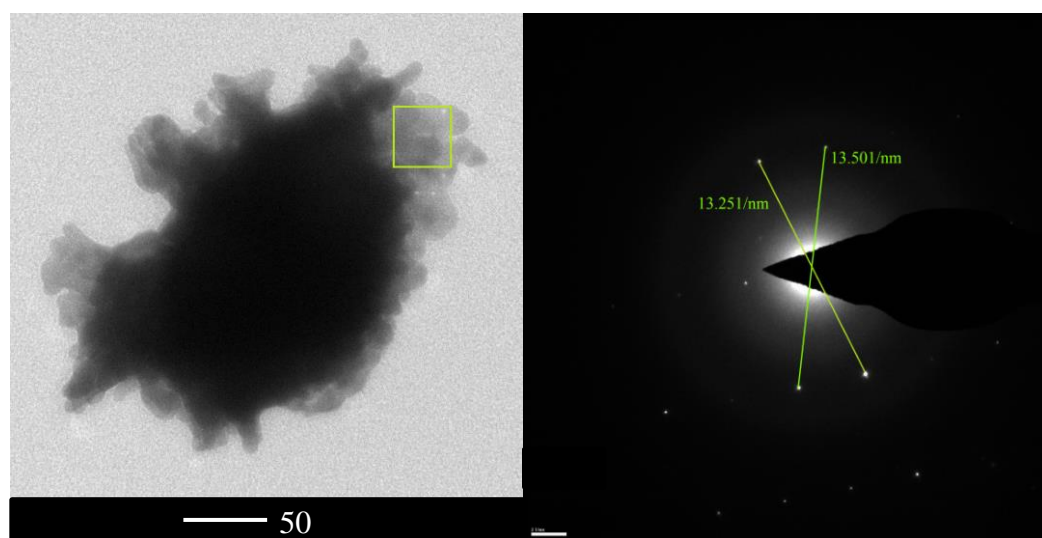
Figure 5. Selected area diffraction pattern for nanoparticles obtained from sample 1 (core-shell nanoparticles).

The SADPs for sample 3 is shown in Figure 6. The diffraction pattern presents a ring arrangement, and the rings were indexed to confirm the crystal structure of the nanoparticles. The index process was done analytically and by running simulations using WebEMAPS. Also, the radii of the rings were measured to calculate the d-spaces of the crystals. Figure 6.a shows the indexed pattern and Figure 6.b shows the radii

measurements of SADPs for BMNPs from sample 3. Table 4 shows the radii (R) of the

diffraction pattern, the ratio (Rn/R1), the obtained diffraction planes and d-spaces.
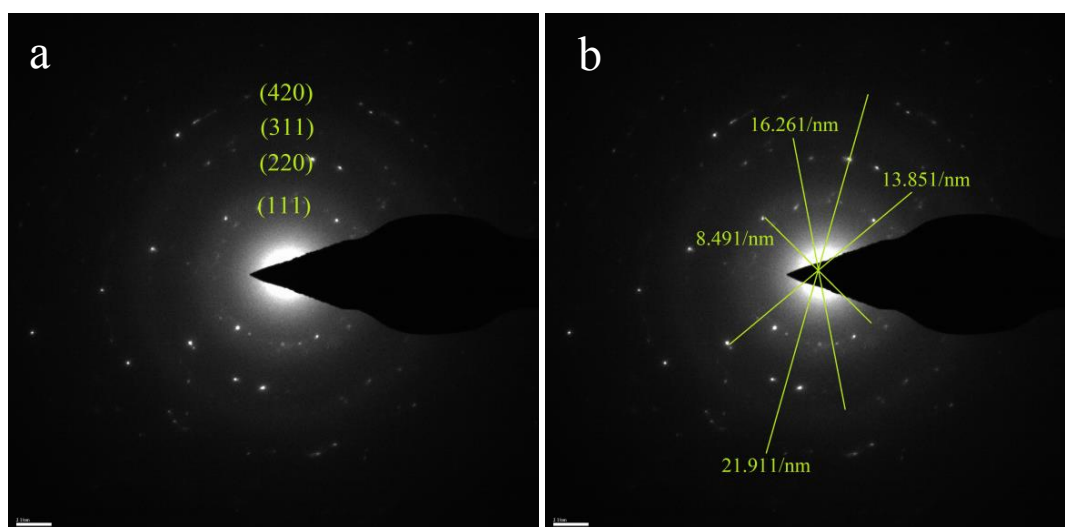
Figure 6. Selected area diffraction pattern of BMNPs from sample 3 (a) indexed
SADP (b) radii measurements.

Table 4. Selected area diffraction pattern analysis for sample 3: radii, ratio (Rn/R1),
diffraction planes and d-spaces.

Ring	Radius (R) [1/nm]	Ratio [Rn/R_1]	Diffraction plane	d-space [Å]
1	4.245 ± 0.001	1.000 ± 0.001	111	2.361 ± 0.001
2	6.925 ± 0.001	1.631 ± 0.001	220	1.441 ± 0.001
3	8.130 ± 0.001	1.915 ± 0.001	311	1.230 ± 0.001
4	10.955 ± 0.001	2.580 ± 0.001	420	0.912 ± 0.001

The four rings in the SADP for the nanoparticles produced with the irradiation of sample 3 correspond to the planes 111, 220, 311, and 420 reflections of the fcc crystal structure with lattice parameter of 4.082 ± 0.001 Å.

According to the data shown in Table 3, this lattice parameter is between the values for Au and Ag lattice parameters (4.078 Å and 4.085 Å respectively) which confirm the production of alloyed Au/Ag bimetallic structure. Since the lattice parameter values for Au and Ag are similar to each other, it is difficult to detect the random replacement of atoms of one element by atoms of another by using the electron diffraction analysis. However, it is possible to affirm that the production of alloy Au/Ag nanoparticles was successfully accomplished in sample 3.

The presence of Cl⁻ in the EDS analysis is due to the chlorine in the gold precursor and the precipitation of AgCl. Additionally, from the SADP analysis it was confirmed that AgCl is not present on the surface of the BMNPs because the lattice parameter for the crystals obtained in sample 3 (4.0816 Å) is smaller than the lattice parameter for AgCl (5.549 Å) and the precipitated particles of AgCl did not interact with the BMNP.

In conclusion, the synthesis of Au/Ag bimetallic nanoparticles was successfully accomplished by water radiolysis for 3 minutes using the MSTR at 10kW of reactor thermal power. Core-shell structures were obtained with the irradiation of solutions with Au/Ag concentrations of 70/30 vol% and 50/50 vol%, and it was found that the shell composition was pure Ag and the core composition was pure Au. Alloyed Au/Ag nanoparticles were obtained with the irradiation of a solution with Au/Ag concentration

of 30/70 vol%. It was confirmed that the alloyed metal nanoparticles presented an fcc crystal structure with a lattice parameter of 4.082 ± 0.001 Å. The EDS analysis showed a composition of the alloyed metal of 70.21 ± 0.01 wt% Au and 28.59 ± 0.01 wt% Ag with uncertainty of 1.32 ± 0.01% and 0.49 ± 0.01% respectively. The presence of precipitated AgCl due to the chemical reactions between both precursors was also detected but this product was not found in the surface of the BMNPs, meaning that they did not act in the synthesis of the BMNPs.

Although the results presented in this work have demonstrated the effectiveness of the synthesis of bimetallic Au/Ag nanoparticles, a further research should be conducted to enhance the production of the nanoparticles by including an inhibitor agent to avoid the precipitation of AgCl. Additionally, future experiments could include the variation of reactor power and irradiation time in order to study the particle size distribution of the BMNPs.

REFERENCES

(1)   A. Shah and R. Qureshi, "Synthesis , Characterization And Applications Of Bimetallic (Au-Ag , Au-Pt , Au-Ru) Alloy Nanoparticles," vol. 30, pp. 133–149, 2012.

(2)   S. M. Roopan, T. V. Surendra, G. Elango, and S. H. S. Kumar, "Biosynthetic trends and future aspects of bimetallic nanoparticles and its medicinal applications," *Appl. Microbiol. Biotechnol.*, vol. 98, no. 12, pp. 5289–5300, 2014.

(3)   H. Nitani, T. Nakagawa, H. Daimon, Y. Kurobe, T. Ono, Y. Honda, A. Koizumi, S. Seino, and T. A. Yamamoto, "Methanol oxidation catalysis and substructure of PtRu bimetallic nanoparticles," *Appl. Catal. A Gen.*, vol. 326, no. 2, pp. 194–201, 2007.

(4)   T. A. Yamamoto, S. Kageyama, S. Seino, H. Nitani, T. Nakagawa, R. Horioka, Y. Honda, K. Ueno, and H. Daimon, "Methanol oxidation catalysis and substructure of PtRu/C bimetallic nanoparticles synthesized by a radiolytic process," *Appl. Catal. A Gen.*, vol. 396, no. 1–2, pp. 68–75, 2011.

(5)   B. Xia, F. He, and L. Li, "Preparation of bimetallic nanoparticles using a facile green synthesis method and their application.," *Langmuir*, vol. 29, no. 15, pp. 4901–7, 2013.

(6)   N. Toshima and T. Yonezawa, "Bimetallic nanoparticles—novel materials for chemical and physical applications," *New J. Chem.*, vol. 22, no. 11, pp. 1179–1201, 1998.

(7)   M. Sharma, P. R. Pudasaini, F. Ruiz-zepeda, E. Vinogradova, and A. a Ayon, "Plasmonic Effects of Au / Ag Bimetallic Multispiked Nanoparticles for Photovoltaic Applications," *ACS Appl. Mater. Interfaces*, vol. 6, pp. 15472–15479, 201.

(8)   J. Belloni, "Nucleation, growth and properties of nanoclusters studied by radiation chemistry: Application to catalysis," *Catal. Today*, vol. 113, no. 3–4, pp. 141–156, 2006.

(9)   M. Treguer, C. De Cointet, H. Remita, J. Khatouri, M. Mostafavi, J. Amblard, J. Belloni, and R. De Keyzer, "Dose Rate Effects on Radiolytic Synthesis of Gold-Silver Bimetallic Clusters in Solution," *J. Phys. Chem. B*, vol. 5647, no. 98, pp. 4310–4321, 1998.

(10)   J. Rojas and C. H. Castano, "Production and Characterization of Supported Transition Metal Nano-Particles on Multi-Walled Carbon Nanotubes Functionalized By Gamma Irradiation and Chemical," in *Materials Processing and Energy Materials*, 2011, vol. 1, pp. 237–244.

(11) S. Le Caër, "Water Radiolysis: Influence of Oxide Surfaces on H$_2$ Production under Ionizing Radiation," *Water*, vol. 3, no. 4, pp. 235–253, 2011.

(12) J. V. Rojas and C. H. Castano, "Production of palladium nanoparticles supported on multiwalled carbon nanotubes by gamma irradiation," *Radiat. Phys. Chem.*, vol. 81, no. 1, pp. 16–21, 2012.

(13) J. Belloni, M. Mostafavi, H. Remita, J.-L. Marignier, and M.-O. Delcourt, "Radiation-induced synthesis of mono- and multi-metallic clusters and nanocolloids," *New J. Chem.*, vol. 22, no. 11, pp. 1239–1255, 1998.

(14) J. Belloni, J.-L. Marignier, M.-O. Delcourt Euverte, M.-L. Hameaux, and M. Lourseau, "Non-Noble Metal Catalytic Micro Aggregates, A Method For Their Preparation And Their Application In The Catalysis Of The Photoreduction Of Water," 1986.

(15) T. M. Nenoff, D. A. Powers, and Z. Zhang, "Alloy Nanoparticle Synthesis Using Ionizing Radiation," 2011.

(16) P. Wu, Y. Gao, H. Zhang, and C. Cai, "Aptamer-Guided Silver − Gold Bimetallic Nanostructures with Highly Active Surface-Enhanced Raman Scattering for Speci fi c Detection and Near-Infrared Photothermal Therapy of Human Breast Cancer Cells," 2012.

(17) N. Misra, J. Biswal, A. Gupta, J. K. Sainis, and S. Sabharwal, "Gamma radiation induced synthesis of gold nanoparticles in aqueous polyvinyl pyrrolidone solution and its application for hydrogen peroxide estimation," *Radiat. Phys. Chem.*, vol. 81, no. 2, pp. 195–200, 2012.

(18) T. Li, H. G. Park, and S. H. Choi, "gamma-Irradiation-induced preparation of Ag and Au nanoparticles and their characterizations," *Mater. Chem. Phys.*, vol. 105, no. 2–3, pp. 325–330, 2007.

(19) M. Liu and P. Guyot-Sionnest, "Mechanism of silver(I)-assisted growth of gold nanorods and bipyramids," *J. Phys. Chem. B*, vol. 109, no. 47, pp. 22192–22200, 2005.

(20) Web Electron Microscopy Applications Software (WebEMAPS), Department of Materials Science and Engineering University of Illinois at Urbana-Champaign, https://mrl.illinois.edu/facilities/center-microanalysis-materials/web-emaps.

APPENDIX

1. SIMULATION OF THE DIFFRACTION PATTERN FOR PURE Ag
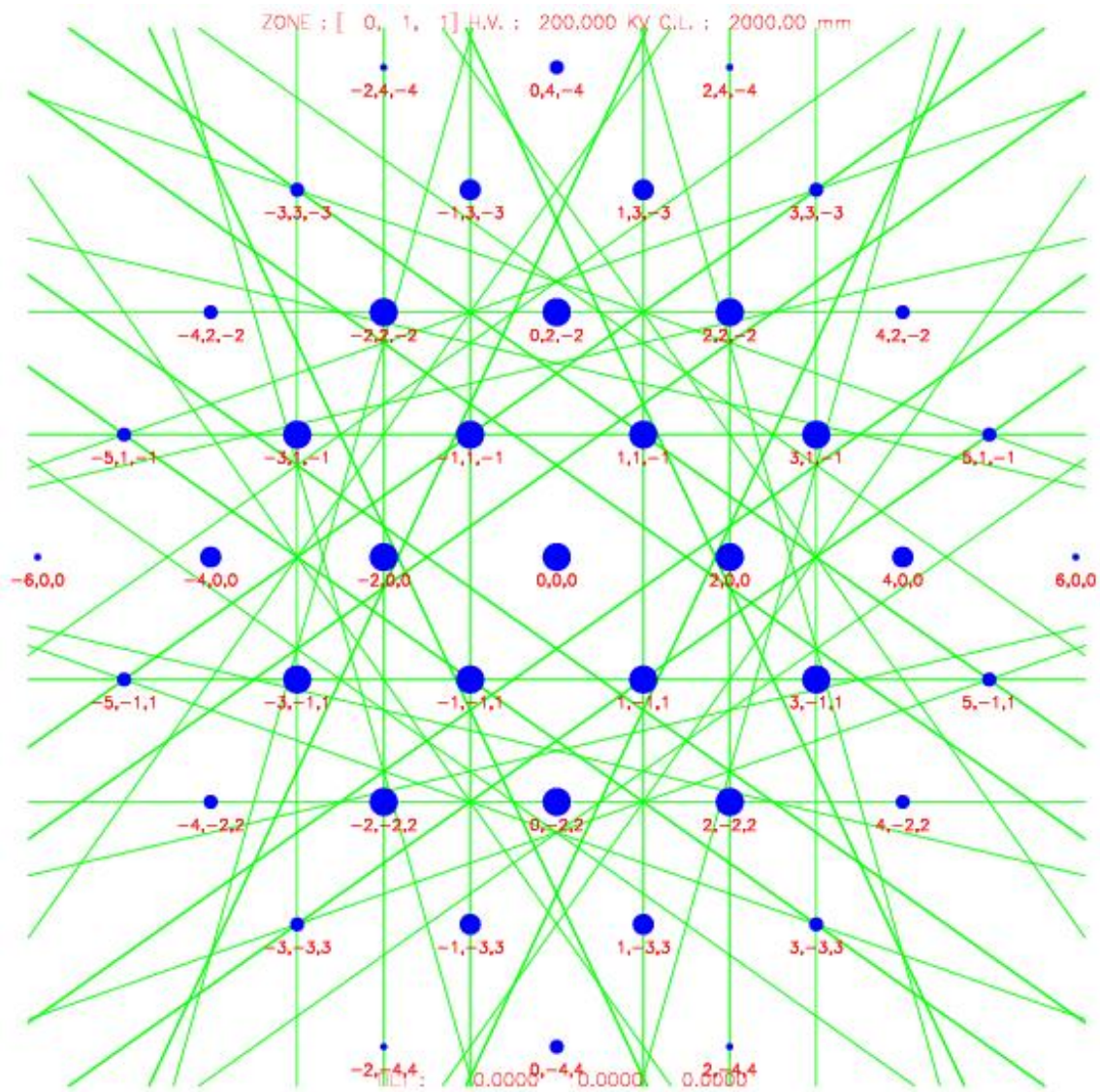
2. SIMULATION OF THE DIFFRACTION PATTERN FOR PURE Au
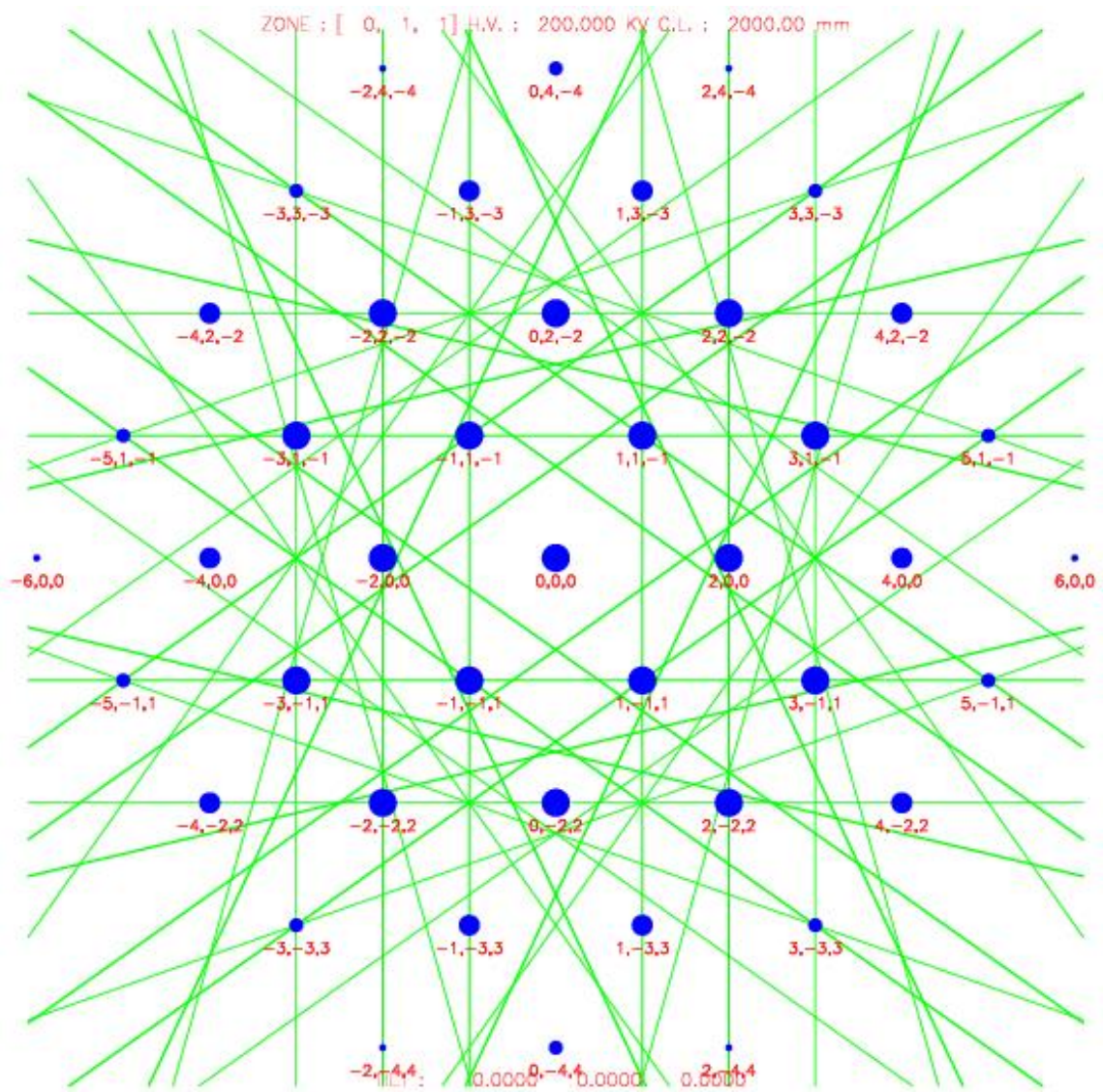
3. SIMULATION OF THE DIFFRACTION PATTERN FOR ALLOYED Au/Ag
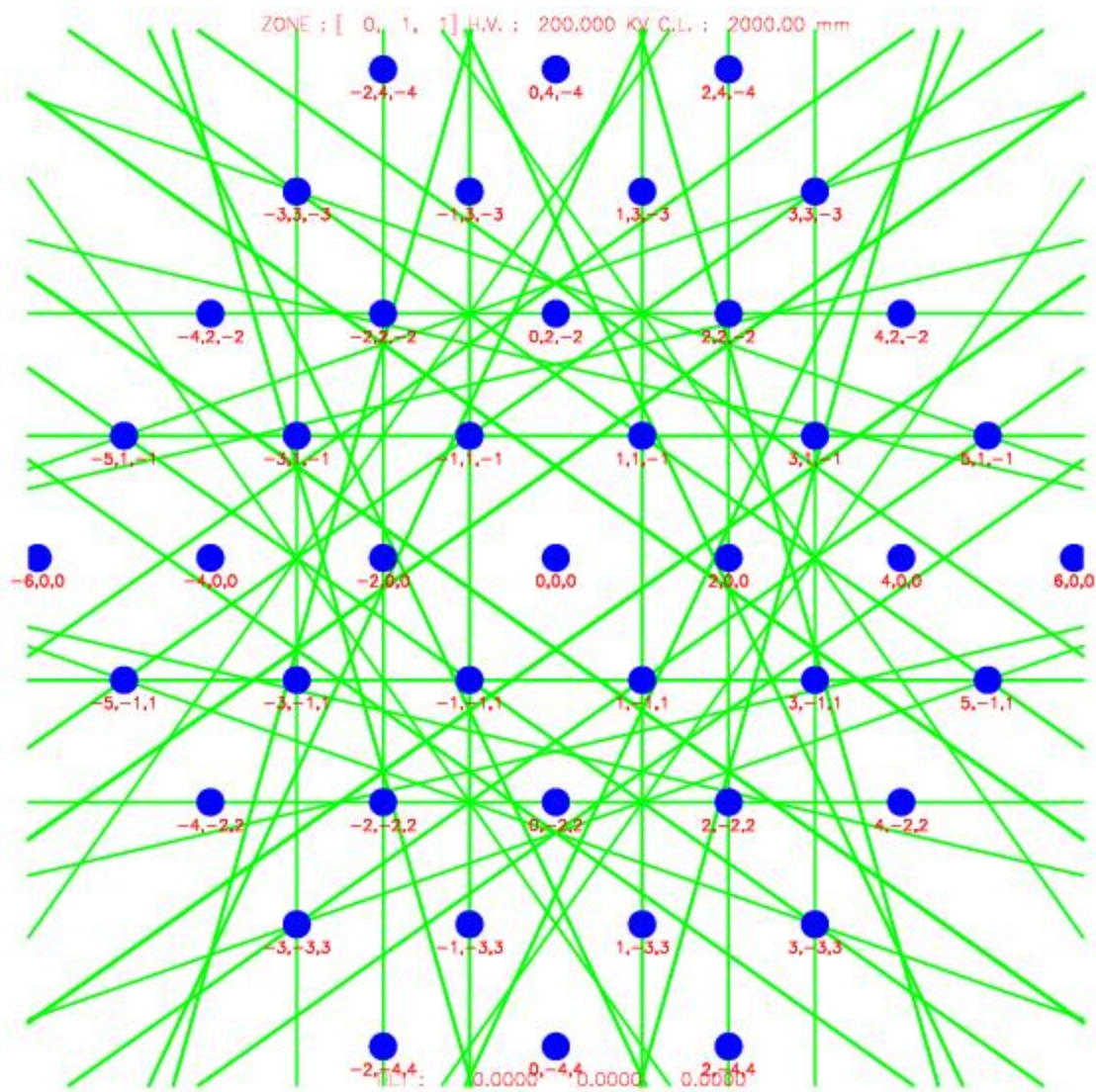
4. SIMULATION OF THE DIFFRACTION PATTERN FOR PURE AgCl
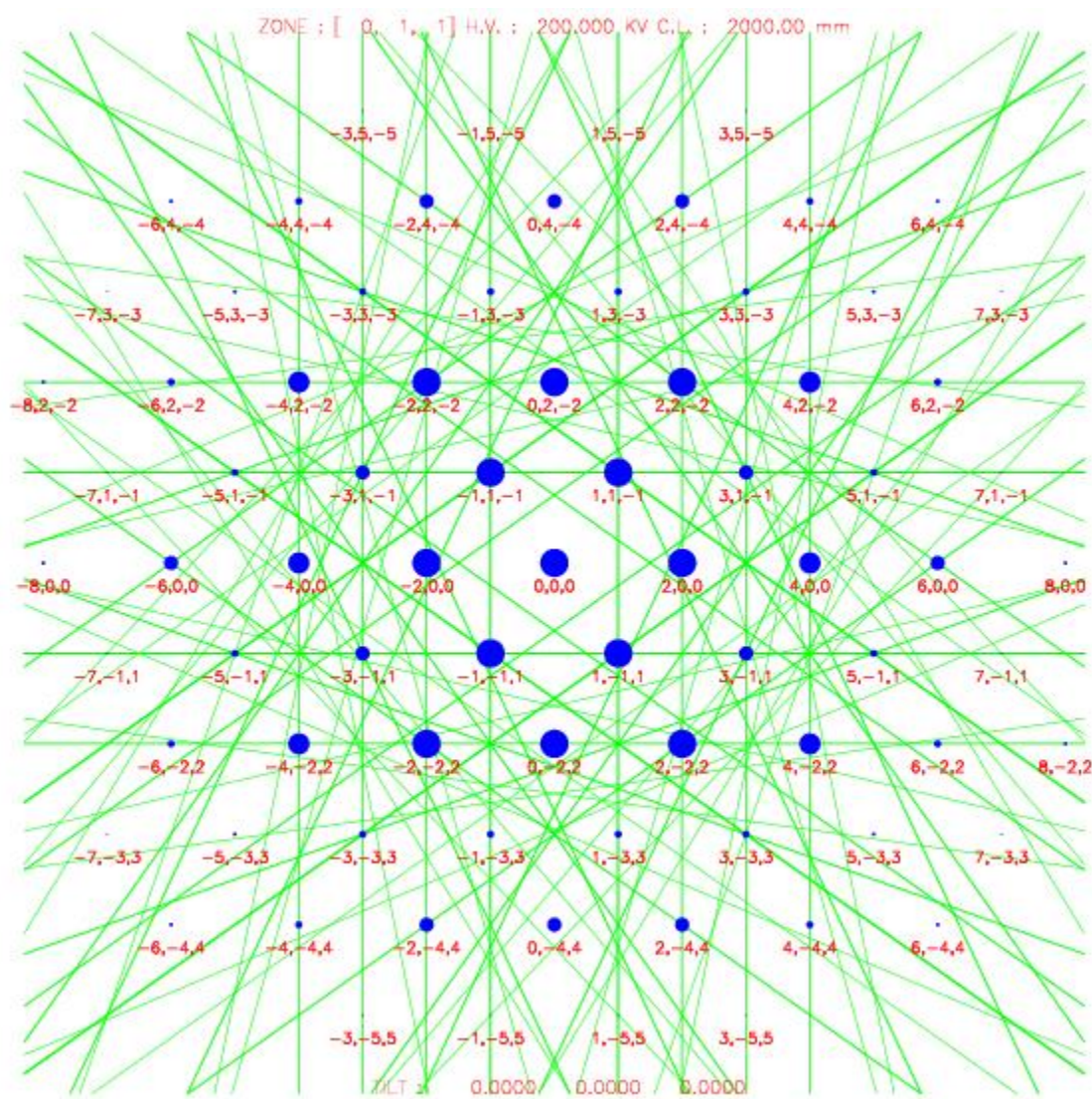
5. DIFFRACTION PLANES AND D-SPACES FOR FCC CRYSTAL STRUCTURE
FOR PURE Ag, PURE Au, AgCl AND ALLOYED Au/Ag FROM SIMULATIONS
USING WEBEMAPS

			Ag- fcc	Au -fcc	AgCl - fcc	Au/Ag - fcc
h	k	l	d[Å]	d[Å]	d[Å]	d[Å]
1	1	1	2.354781	2.354954	3.203717	2.359053
0	0	2	2.039300	2.039450	2.774500	2.043000
0	2	2	1.442003	1.442109	1.961868	1.444619
1	1	3	1.229744	1.229835	1.673086	1.231975
2	2	2	1.177390	1.177477	1.601858	1.179527
0	0	4	1.019650	1.019725	1.387250	1.021500
1	3	3	0.935695	0.935764	1.273028	0.937393
0	2	4	0.912003	0.912070	1.240794	0.913657
2	2	4	0.832541	0.832602	1.132685	0.834051
1	1	5	0.784927	0.784985	1.067906	0.786351
3	3	3	0.784927	0.784985	1.067906	0.786351
0	4	4	0.721001	0.721054	0.980934	0.722310
1	3	5	0.689409	0.689460	0.937952	0.690660
2	4	4	0.679767	0.679817	0.924833	0.681000
0	0	6	0.679767	0.679817	0.924833	0.681000

6. Rn/R1 VALUES FOR DIFFERENT DIFFRACTION PLANES OF THE CUBIC STRUCTURES

hkl	M	SC Rn/R1	bcc Rn/R1	fcc Rn/R1	Diamond Rn/R1
100	1	1			
110	1.414	1.414	1		
111	1.732	1.732		**1**	1
200	2	2	1.414	**1.155**	
210	2.236	2.236			
211	2.449	2.449	1.732		
220	2.828	2.828	2	**1.633**	1.633
300	3	3			
310	3.162	3.162	2.236		
311	3.317	3.317		**1.915**	1.915
222	3.464	3.464	2.449	2	
320	3.606	3.606			
321	3.742	3.742	2.646		
400	4	4	2.828	**2.309**	2.309
410	4.123	4.123			
411	4.243	4.243	3		
311	4.359	4.359		2.517	2.517
420	4.472	4.472	3.162	**2.582**	

SECTION

6. SUMMARY OF RESULTS

6.1. SYNTHESIS OF RADIOACTIVE GOLD NANOPARTICLES USING A RESEARCH NUCLEAR REACTOR

Radioactive AuNPs were successfully synthesized, in a single step, by radiolysis of water using neutron radiation and ionizing radiation. The irradiation process was conducted at 200kW of thermal power using different irradiation times (0.5, 1, 3, 5, 10, 30, and 60 minutes). The average sizes of the obtained nanoparticles ranged from 3 nm to 400 nm. It was found that the particle size and its standard deviation decreased with longer irradiation time following a power trend of 0.968 with R-square 0.996.

The appropriate conditions to produce radioactive AuNPs to be used in cancer treatment were determined (irradiation at 200kW and 10 minutes). The obtained nanoparticles by using these conditions presented an average size of 56 nm with standard deviation 34 nm. The 32% of the nanoparticles obtained with these conditions presented a preferred particle size between 40nm and 60 nm.The chemical composition obtained was 71.7 wt% of Au and 28.7 wt% of Cl, it demonstrates the effective reduction of gold to produce metallic nanoparticles.

6.2. THEORETICAL ESTIMATION OF THE TOTAL ABSORBED DOSE IN MSTR

The theoretical estimation of the total absorbed dose in the MSTR during the production of radioactive AuNPS was achieved. The estimation process was developed by using analytical calculations following the process described by Martinho [1], and by MCNP simulations. The obtained kerma rate due to neutrons was 82.84 Gy/s (29.82

Mrad/h). The obtained gamma dose rate was 36.41 Gy/s (13.10 Mrad/h). The obtained

total absorbed dose rate for the production of radioactive AuNPs at 200kW of thermal

power was 119.25 Gy/s (42.93 Mrad/h) where the gamma dose rate contributes 30.53 %

and the neutron kerma rate contributes 69.47% in the final result.

6.3. PRODUCTION OF BIMETALLIC GOLD – SILVER NANOPARTICLES IN A RESEARCH NUCLEAR REACTOR

Radioactive Au/Ag BMNPs were successfully synthesized by water radiolysis

using neutron radiation and ionizing radiation. The irradiation process was conducted at

10 kW and 3 minutes, four different samples with Au/Ag composition of 70/30 vol%,

50/50 vol%, 70/30 vol%, and 0/100 vol% were irradiated. The production of core-shell

nanoparticles was obtained from samples with Au/Ag concentrations of 70/30 vol% and

50/50 vol%.It was found that the chemical composition of these nanoparticles consisted

on pure Au in the core coated by pure Ag. The production of alloyed Au/Ag

nanoparticles was obtained from samples with Au/Ag concentration of 30/70 vol%, it

was confirmed that these nanoparticles presented a fcc crystal structure with a lattice

parameter of 4.082 ± 0.001 Å. The EDS analysis showed a composition of the alloyed

metal of 70.21 ± 0.01 wt% Au and 28.59 ± 0.01 wt% Ag with uncertainty of 1.32 ±

0.01% and 0.49 ± 0.01% respectively. The presence of precipitated AgCl due to the

chemical reactions between both precursors was also detected but this product was not

found in the surface of the BMNPs, meaning that they did not act in the synthesis of the

BMNPs.

7. CONCLUSIONS

The development of an effective method to produce radioactive nanoparticles in a single step was successfully accomplished. The synthesis process was achieved by reducing the metallic ions present in aqueous solutions by using the products obtained from water radiolysis.

The innovation of this work is the application of neutron radiation and ionizing radiation at the same time to be initiators of water radiolysis. Using both kind of irradiation, it is possible to produce radioactive nanostructures in a single step.

It was possible to produce radioactive AuNPs with stable chemical composition and appropriate conditions to be used in imaging diagnosis and cancer radiation treatment. Furthermore, the production of Au/Ag BMNPs with core-shell and alloyed metal structure was successfully achieved. During this research, it was possible to determine the crystal structure of the alloyed metal nanoparticles.

As additional work, the theoretical total absorbed dose in the MSTR was for the first time estimated. The calculations were conducted by analytical process and by MCNP simulations. It was possible to determine the total absorbed dose during the production of radioactive AuNPs. This study represents the complement of an extensive research of the radioactive behavior of the MSTR.

8. SUGGESTION FOR FUTURE WORK

This work exhibited the potential of the neutron radiation and ionizing radiation to produce radioactive nanostructures in a single step. Also, it was confirmed that the synthesis of radioactive alloyed nanoparticles with defined crystal structure and stable chemical composition.

A further research from this study may be the application of different radiation types to synthesize combined nanostructures (such as nanotubes decorated with nanoparticles) that can be used in medical and heat transfer applications.

Aside from the good results obtained with the BMNPs, a future work may include the production of radioactive and non-radioactive multimetallic nanoparticles with appropriated characteristics and crystal structures that could represent a novel nanomaterial for imaging diagnosis and cancer treatment.

Additionally, a further work from this thesis may be the validation of the theoretical estimation of the total absorbed dose by MCNP simulation and experimental work.

BIBLIOGRAPHY

[1] E. Drexler, *Engines of Creaction: The Coming Era of Nanotechnology*. 1986.

[2] "National Nanotechnology Initiative." [Online]. Available: http://www.nano.gov/.

[3] M. Kuno, *Introduction to Nanoscience and Nanotechnology: A Workbook*. 2004.

[4] M. H. Fulekar, *Nanotechnology: Importance and Applications*. New Delhi: I.K International Pub. House, 2010.

[5] X. Ma, X. Zhang, X. Guo, Q. Kang, D. Shen, and G. Zou, "Sensitive and selective determining ascorbic acid and activity of alkaline phosphatase based on electrochemiluminescence of dual-stabilizers-capped CdSe quantum dots in carbon nanotube-nafion composite," *Talanta*, vol. 154, pp. 175–182, 2016.

[6] S. Chen, Y. Song, F. Shi, Y. Liu, and Q. Ma, "Sensitive detection of picric acid based on creatinine-capped solid film assembled by nitrogen-doped graphene quantum dots and chitosan," *Sensors Actuators B Chem.*, vol. 231, pp. 634–640, 2016.

[7] Y. Wang, J. Chen, B. Yang, H. Qiao, L. Gao, T. Su, S. Ma, X. Zhang, X. Li, G. Liu, J. Cao, X. Chen, Y. Chen, and F. Cao, "*In vivo* MR and Fluorescence Dual-modality Imaging of Atherosclerosis Characteristics in Mice Using Profilin-1 Targeted Magnetic Nanoparticles," *Theranostics*, vol. 6, no. 2, pp. 272–286, 2016.

[8] R. Chaudhary, K. Roy, R. K. Kanwar, K. Walder, and J. R. Kanwar, "Engineered atherosclerosis-specific zinc ferrite nanocomplex-based MRI contrast agents," *J. Nanobiotechnology*, vol. 14, no. 1, p. 6, 2016.

[9] N. Gao, "Gold-Nanoparticle-Based Multifunctional Amyloid-β Inhibitor against Alzheimer's Disease," *Chem. a Eur. J.*, vol. 21, no. 2, pp. 829–835, 2015.

[10] A. de la Escosura-Muñiz, Z. Plichta, D. Horák, and A. Merkoçi, "Alzheimer's disease biomarkers detection in human samples by efficient capturing through porous magnetic microspheres and labelling with electrocatalytic gold nanoparticles," *Biosens. Bioelectron.*, vol. 67, pp. 162–169, 2015.

[11] S. Papa, F. Rossi, R. Ferrari, A. Mariani, M. De Paola, I. Caron, F. Fiordaliso, C. Bisighini, E. Sammali, C. Colombo, M. Gobbi, M. Canovi, J. Lucchetti, M. Peviani, M. Morbidelli, G. Forloni, G. Perale, D. Moscatelli, and P. Veglianese, "Selective nanovector mediated treatment of activated proinflammatory microglia/macrophages in spinal cord injury," *ACS Nano*, vol. 7, no. 11, pp. 9881–9895, 2013.

[12]   Y. Cho and R. Ben Borgens, "Polymer and nano-technology applications for repair and reconstruction of the central nervous system," *Exp. Neurol.*, vol. 233, no. 1, pp. 126–144, 2012.

[13]   J. R. Kanwar, *Cancer nanotechnology*, vol. 4, no. 1. 2012.

[14]   World Health Organization, "Global status report on noncommunicable diseases 2010," *World Health*, p. 176, 2010.

[15]   R. Siegel, K. Miller, and A. Jemal, "Cancer statistics , 2015 .," *CA Cancer J Clin*, vol. 65, no. 1, p. 29, 2015.

[16]   J. V. Jokerst and S. S. Gambhir, "Molecular imaging with theranostic nanoparticles," *Acc. Chem. Res.*, vol. 44, pp. 1050–1060, 2011.

[17]   P. Debbage and W. Jaschke, "Molecular imaging with nanoparticles: Giant roles for dwarf actors," *Histochem. Cell Biol.*, vol. 130, pp. 845–875, 2008.

[18]   E. I. Altinoglu and J. H. Adair, "Near infrared imaging with nanoparticles," *Wiley Interdiscip. Rev. Nanomedicine Nanobiotechnology*, vol. 2, pp. 461–477, 2010.

[19]   X. He, K. Wang, and Z. Cheng, "In vivo near-infrared fluorescence imaging of cancer with nanoparticle-based probes," *Wiley Interdiscip. Rev. Nanomedicine Nanobiotechnology*, vol. 2, pp. 349–366, 2010.

[20]   V. Ntziachristos, "Going deeper than microscopy: The optical imaging frontier in biology," *Nat. Methods*, vol. 7, pp. 603–614, 2010.

[21]   W. E. Doering, E. Piotti, M. J. Natan, and E. Al, "SERS as a foundation for nanoscale, optically detected biological labels," *Adv. Mater.*, vol. 19, pp. 3100–3108, 2007.

[22]   L. V. Wang, "Multiscale photoacoustic microscopy and computed tomography," *Nat. Photonics*, vol. 3, pp. 503–509, 2009.

[23]   M. Hahn, A. Singh, and P. Sharma, "Nanoparticles as contrast agents for in-vivo bioimaging: Current status and future prespectives," *Anal. Bioanal. Chem.*, vol. 300, pp. 3–27, 2010.

[24]   N. Becker, D. Liebermann, H. Wesch, and E. Al., "Mortality among Thorotrast-exposed patients and an unexposed comparison group in the German Thorotrast study," *Eur. J. Cancer*, vol. 44, pp. 1259–1268, 2008.

[25]   P. A. Jackson, W. N. Rahman, C. J. Wong, and E. Al, "Potential dependet superiority of gold nanoparticles in comparison to iodinated contrast agents," *Eur. J. Radiol.*, vol. 75, pp. 104–109, 2010.

[26] L. E. Jennings and N. J. Long, "'Two is better than one' -Probes for dual-modality molecular imaging," *Chem. Commun.*, vol. 24, pp. 3511–3524, 2009.

[27] S. A. Wickline, A. M. Neubauer, P. M. Winter, and E. Al, "Molecular imaging and therapy of atherosclerosis with targeted nanoparticles," *J. Magn. Reson. Imaging JMRI*, vol. 25, pp. 667–680, 2007.

[28] Z.-J. Zheng, J. B. Croft, W. H. Giles, and G. A. Mensah, "Sudden Cardiac Death in the United States, 1989 to 1998," *Circulation*, vol. 104, no. 18, pp. 2158–2163, Oct. 2001.

[29] G. Mie, "Considerations on the optics of turbid media, specially colloidal metal sols," *Ann. Phys.*, vol. 25, pp. 377–442, 1908.

[30] P. K. Jain, X. Huang, I. H. El-Sayed, and M. A. El-Sayed, "Noble metals on the nanoscale: Optical and photothermal properties and some applications in imaging, sensing, biology, and medicine," *Acc. Chem. Res.*, vol. 41, pp. 1578–1586, 2008.

[31] U. Kreibig and M. Vollmer, *Optical Properties of Metal Clusters*, 1st ed. Base,l Switzerland: Springer-Verlag Berlin Heidelberg, 1995.

[32] P. K. Jain, K. S. Lee, I. H. El-Sayed, and M. A. El-Sayed, "Calculated absorption and scattering properties of gold nanoparticles of different size, shape, and composition: Applications in biological imaging and biomedicine," *J. Phys. Chem. B*, vol. 110, pp. 7238–7248, 2006.

[33] K. L. Kelly, E. Coronado, L. L. Zhao, and G. C. Schatz, "The optical properties of metal nanoparticles: The influence of size, shape, and dielectric environment," *J. Phys. Chem. B*, vol. 107, pp. 668–677, 2003.

[34] E. E. Connor, J. Mwamuka, A. Gole, C. J. Murphy, and M. D. Wyatt, "Gold Nanoparticles are Taken Up by Human Cells but Do Not Causes Acute Cytotoxicity," *Small*, vol. 1, no. 3, pp. 325–327, 2005.

[35] T. S. Hauck, A. A. Ghazani, and W. C. W. Chan, "Assessing the Effect of Surface Chemistry on Gold Nanorod Uptake, Toxicity, and Gene Expression in Mammalian Cells," *Small*, vol. 4, no. 1, pp. 153–159, 2008.

[36] P. H. Davis, C. P. Morrisey, S. M. V Tuley, and C. I. Bingham, "Synthesis and Stabilization of Colloidal Gold Nanoparticle Suspensions For SERS," *Nanoparticles Synth. Stab. Passiv. Funct.*, vol. 996, no. 16, pp. 16–30, 2008.

[37] M. Hu, J. Chen, Z. J. Li, L. Au, G. V. Hartland, X. Li, M. Marquez, and Y. Xia, "Gold nanostructures: Engineering their plasmonic properties for biomedical applications," *Chem. Soc. Rev.*, vol. 35, no. 11, pp. 1084–1094, 2006.

[38] J. Kimling, M. Maier, B. Okenve, V. Kotaidis, H. Ballot, and A. Plech, "Turkevich method for gold nanoparticles synthesis revisited," *J. Phys. Chem. B*, vol. 110, no. 32, pp. 15700–15707, 2006.

[39] J. Turkevich, P. C. Stevenson, and J. Hillier, "A study of the nucleation and growth processes in the synthesis of colloidal gold," *Discuss. Farady Soc.*, vol. 11, pp. 55–75, 1951.

[40] S. J. Oldenburg, J. B. Jackson, S. L. Westcott, and N. J. Halas, "Infrared extinction properties of gold nanoshells," *Appl. Phys. Lett.*, vol. 75, no. 19, pp. 2897–2899, 1999.

[41] S. J. Oldenburg, R. D. Averitt, S. L. Westcott, and N. J. Halas, "Nanoengineering of optical resonances," *Chem. Phys. Lett.*, vol. 288, pp. 243–247, 1998.

[42] K. Welsher, Z. Liu, S. P. Sherlock, and E. Al, "A route to brightly fluorescent carbon nanotubes for near-infrared imaging in mice," *Nat. Nanotechnol.*, vol. 4, pp. 773–780, 2009.

[43] I. J. Das, "Forward dose perturbation at high atomic number interfaces in kilovoltage x-ray beams," *Med. Phys.*, vol. 24, pp. 1781–1787, 1997.

[44] I. J. Das and K. L. Chopra, "Backscatter dose perturbation in kilovoltage photon beams at high atomic number interfaces," *Med. Phys.*, vol. 22, pp. 767–773, 1995.

[45] H. Matsudaira, A. M. Ueno, and I. Furuno, "Iodine Contrast Medium Sensitizes Cultured Mammalian Cells to X Rays but Not to γ Rays," *Radiat. Res.*, vol. 84, pp. 144–148, 1980.

[46] R. S. Mello, H. Callisen, J. Winter, A. R. Kagan, and A. Norman, "Radiation dose enhancement in tumors with iodine," *Med. Phys.*, vol. 10, pp. 75–78, 1983.

[47] M. H. Castillo, T. M. Button, R. Doerr, M. I. Homs, C. W. Pruett, and J. I. Pearce, "Effects of radiotherapy on mandibular reconstruction plates," *Am. J. Surg.*, vol. 156, pp. 261–263, 1988.

[48] D. F. Regulla, L. B. Hieber, and M. Seidenbusch, "Physical and biological interface dose effects in tissue doe to x-ray-induced release of secondary radiation from metallic gold surface," *Radiat. Res.*, vol. 150, pp. 92–100, 1998.

[49] A. Anshup, J. S. Venkataraman, C. Subramaniam, R. R. Kumar, S. Priya, T. R. S. Kumar, R. V. Omkumar, A. John, and T. Pradeep, "Growth of gold nanoparticles in human cells," *Langmuir*, vol. 21, pp. 11562–11567, 2005.

[50] T. Niidome, K. Nakashima, H. Takahashi, and Y. Niidome, "Preparation of primary amine-modified gold nanoparticles and their trasfection ability into cultivated cells," *Chem. Commun.*, vol. 17, pp. 1978–1979, 2004.

[51] E. A. Foley, J. D. Carter, F. Shan, and T. Guo, "Enhanced relaxation of nanoparticles-bound supercoiled DNA in x-ray radiation," *Chem. Commun.*, vol. 7, no. 25, pp. 3192–3194, 2005.

[52] K. T. Butterworth, J. A. Wyer, M. Brennan-Fournet, C. J. Latimer, M. B. Shah, F. J. Currell, and D. G. Hirst, "Variation of strand break yield for plasmid DNA irradiated with high-Z metal nanoparticles," *Radiat. Res.*, vol. 170, pp. 381–387, 2008.

[53] K. T. Butterworth, J. A. Coulter, S. Jain, J. Forker, S. J. Mcmahon, G. Schettino, F. J. Currell, and D. G. Hirst, "UKPMC Funders Group nm gold particles : potential application for cancer therapy," *Evaluation*, vol. 21, no. 29, 2011.

[54] M. Y. Chang, A. L. Shiau, Y. H. Chen, C. J. Chang, H. H. W. Chen, and C. L. Wu, "Increased apoptotic potential and dose-enhancing effect of gold nanoparticles in combination with single-dose clinical electron beams on tumor-bearing mice," *Cancer Sci.*, vol. 99, pp. 1479–1484, 2008.

[55] J.-K. Kim, S.-J. Seo, K.-H. Kim, and E. Al, "Therapeutic application of metallic nanoparticles combined with particle-induced x-ray emission effect," *Nanotechnology*, vol. 21, no. 42, p. 425102, 2010.

[56] C. M. Spencer and K. L. Goa, "Amifostine. A review of its pharmacodynamic and pharmacokinetic properties, and therapeutic potential as a radioprotector and cytotoxic chemoprotector," *Drugs*, vol. 50, no. 6, pp. 1001–1031, 1995.

[57] R. W. Tarnuzzer, J. Colon, and E. Al, "Vacancy engineered ceria nanostructures for protection from radiation-induced celular damage," *Nano Lett.*, vol. 5, no. 12, pp. 2573–2577, 2005.

[58] P. J. Krusic, E. Wasserman, and E. Al, "Radical reactions of C60," *Science (80-.).*, vol. 254, no. 5035, pp. 1183–1185, 1991.

[59] L. L. Dugan, J. K. Gabrielesen, and E. Al, "Buckminsterfullerenol free radical scavengers reduce excitotoxic and apoptotic death of cultured cortical neurons," *Neurobiol. Dis.*, vol. 3, no. 2, pp. 129–135, 1996.

[60] "Cancer Treatment Centers of America." [Online]. Available: http://www.brachytherapy.com/.

[61] B. Thomadsen, M. J. Rivard, and W. M. Butler, Eds., *Brachytherapy Physics*, 2nd ed. Madison, WI: American Association of Physicists in Medicine by Medical Physics Pub., 2005.

[62] F. M. Khan, *The Physics of Radiation Therapy*, 3rd. ed. Philadelphia, PA: Lippincott Williams & Wilkins, 2003.

[63] K. V. Katti, R. Kannan, K. Katti, V. Kattumuri, R. Pandrapragada, V. Rahing, C. Cutler, E. J. Boote, S. W. Casteel, C. J. Smith, and E. Al, "Hybrid gold nanoparticles in molecular imaging and radiotherapy," *Czechoslov. J. Phys.*, vol. 56, no. 1, pp. d23–d34, 2006.

[64] N. Chanda, V. Kattumuri, R. Shukla, A. Zambre, K. Katti, A. Upendran, R. R. Kulkarni, P. Kan, G. M. Fent, S. W. Casteel, and E. Al, "Bombesin functionalized gold nanoparticles show in vitro and in vivo cancer receptor specificity," in *Proceedings of the National Academy of Sciences of the United States of America*, 2010, pp. 8760–8765.

[65] N. Chanda, P. Kan, L. D. Watkinson, R. Shukla, A. Zambre, T. L. Carmack, H. Engelbrecht, J. R. Lever, K. Katti, G. M. Fent, S. W. Casteel, C. J. Smith, W. H. Miller, S. Jurisson, E. Boote, J. D. Robertson, C. Cutler, M. Dobrovolskaia, R. Kannan, and K. V. Katti, "Radioactive gold nanoparticles in cancer therapy: therapeutic efficacy studies of GA-198AuNP nanoconstruct in prostate tumor-bearing mice," *Nanomedicine Nanotechnology, Biol. Med.*, vol. 6, no. 2, pp. 201–209, 2010.

[66] R. Kannan, V. Rahing, C. Cutler, R. Pandrapragada, K. K. Katti, V. Kattumuri, J. D. Robertson, S. J. Casteel, S. Jurisson, C. Smith, E. Boote, and K. V. Katti, "Nanocompatible chemistry toward fabrication of target-specific gold nanoparticles," *J. Am. Chem. Soc.*, vol. 128, no. 35, pp. 11342–11343, 2006.

[67] R. H. Flocks, H. D. Kerr, H. B. Elkins, and D. Culp, "The treatment of carcinoma of the prostate by interstitial radiation with radio-active gold (Au198): A preliminary report," *J. Urol.*, vol. 68, no. 2, pp. 510–522, 1952.

[68] R. H. Flocks, H. D. Kerr, H. B. Elkins, and D. Culp, "The treatment of carcinoma of the prostate by interstitial radiation with radiactive gold (Au 198): A follow-up report," *J. Urol.*, vol. 71, no. 5, pp. 628–633, 1954.

[69] G. J. Bulkey and V. J. O'Conor, "Treatment of carcinoma of the prostate by interstitial irradiation with radioactive gold. Experimental and clinical studies," *Trans. Am. Assoc. Genitourin. Surg.*, vol. 51, pp. 126–133, 1959.

[70] M. Patyanik, A. Mayer, and I. Polgar, "Results of Ovary Tumor Treatment With Abdominally Administered 198Au Evaluated on the Basis of Long Term Follow Up," *Pathol. oncolgy Res.*, vol. 8, no. 1, pp. 54–57, 2002.

[71] L. P. Balogh, S. S. Nigavekar, A. C. Cook, L. Minc, and M. K. Khan, "Development of dendrimer-gold radioactive nanocomposites to treat cancer microvasculature," *PharmaChem*, vol. 2, no. 4, pp. 94–99, 2003.

[72] M. C. Daniel and D. Astruc, "Gold Nanoparticles: Assembly, Supramolecular Chemistry, Quantum-Size-Related Properties, and Applications Toward Biology, Catalysis, and Nanotechnology," *Chem. Rev.*, vol. 104, no. 1, pp. 293–346, 2004.

[73] P. J. G. Goulet and R. B. Lennox, "New insights into Brust-Schiffrin metal nanoparticle synthesis," *J. Am. Chem. Soc.*, vol. 132, no. 28, pp. 9582–9584, 2010.

[74] D. M. Herold, I. J. Das, C. C. Stobbe, R. V Iyer, and J. D. Chapman, "Gold microspheres: a selective technique for producing biologically effective dose enhancement.," *Int. J. Radiat. Biol.*, vol. 76, no. 10, pp. 1357–1364, 2000.

[75] S. K. Nune, N. Chanda, R. Shukla, K. Katti, R. R. Kulkarni, S. Thilakavathy, S. Mekapothula, R. Kannan, and K. V. Katti, "Green nanotechnology from tea: phytochemicals in tea as building blocks for production of biocompatible gold nanoparticles," *J. Mater. Chem.*, vol. 19, no. 19, p. 2912, 2009.

[76] A. Shah and R. Qureshi, "Synthesis , Characterization And Applications Of Bimetallic (Au-Ag , Au-Pt , Au-Ru) Alloy Nanoparticles," vol. 30, pp. 133–149, 2012.

[77] J. Li, J. Wu, X. Zhang, Y. Liu, D. Zhou, H. Sun, H. Zhang, and B. Yang, "Controllable synthesis of stable urchin-like gold nanoparticles using hydroquinone to tune the reactivity of gold chloride," *J. Phys. Chem. C*, vol. 115, no. 9, pp. 3630–3637, 2011.

[78] J. Belloni, "Nucleation, growth and properties of nanoclusters studied by radiation chemistry: Application to catalysis," *Catal. Today*, vol. 113, no. 3–4, pp. 141–156, 2006.

[79] J. Belloni, M. Mostafavi, H. Remita, J.-L. Marignier, and M.-O. Delcourt, "Radiation-induced synthesis of mono- and multi-metallic clusters and nanocolloids," *New J. Chem.*, vol. 22, no. 11, pp. 1239–1255, 1998.

[80] A. I. El-Batal, A.-A. M. Hashem, and N. M. Abdelbaky, "Gamma radiation mediated green synthesis of gold nanoparticles using fermented soybean-garlic aqueous extract and their antimicrobial activity.," *Springerplus*, vol. 2, no. 1, p. 129, 2013.

[81] T. Li, H. G. Park, and S. H. Choi, "gamma-Irradiation-induced preparation of Ag and Au nanoparticles and their characterizations," *Mater. Chem. Phys.*, vol. 105, no. 2–3, pp. 325–330, 2007.

[82] N. Misra, J. Biswal, A. Gupta, J. K. Sainis, and S. Sabharwal, "Gamma radiation induced synthesis of gold nanoparticles in aqueous polyvinyl pyrrolidone solution and its application for hydrogen peroxide estimation," *Radiat. Phys. Chem.*, vol. 81, no. 2, pp. 195–200, 2012.

[83] J. Rojas and C. H. Castano, "Production and Characterization of Supported Transition Metal Nano-Particles on Multi-Walled Carbon Nanotubes Functionalized By Gamma Irradiation and Chemical," in *Materials Processing and Energy Materials*, 2011, vol. 1, pp. 237–244.

[84] R. Kannan, A. Zambre, N. Chanda, R. Kulkarni, R. Shukla, K. Katti, A. Upendran, C. Cutler, E. Boote, and K. V. Katti, "Functionalized radioactive gold nanoparticles in tumor therapy," *Wiley Interdiscip. Rev. Nanomedicine Nanobiotechnology*, vol. 4, no. 1, pp. 42–51, 2012.

[85] W. Wang, Z. Yu, and W. Su, "Ion irradiation and biomolecular radiation damage II. Indirect effect," *arXiv*, no. 1, p. 8, 2010.

[86] T. E. Schmid, G. Dollinger, V. Hable, C. Greubel, O. Zlobinskaya, D. Michalski, M. Molls, and B. R??per, "Relative biological effectiveness of pulsed and continuous 20 MeV protons for micronucleus induction in 3D human reconstructed skin tissue," *Radiother. Oncol.*, vol. 95, no. 1, pp. 66–72, 2010.

[87] A. Maquille, J. L. H. Jiwan, and B. Tilquin, "Radiosterilization of drugs in aqueous solutions may be achieved by the use of radioprotective excipients," *Int. J. Pharm.*, vol. 349, no. 1–2, pp. 74–82, 2008.

[88] T. Katayama, M. Nakauma, S. Todoriki, G. O. Phillips, and M. Tada, "Radiation-induced polymerization of gum arabic (Acacia senegal) in aqueous solution," *Food Hydrocoll.*, vol. 20, no. 7, pp. 983–989, 2006.

[89] S. Le Caër, "Water Radiolysis: Influence of Oxide Surfaces on H2 Production under Ionizing Radiation," *Water*, vol. 3, no. 4, pp. 235–253, 2011.

[90] J. V. Rojas and C. H. Castano, "Production of palladium nanoparticles supported on multiwalled carbon nanotubes by gamma irradiation," *Radiat. Phys. Chem.*, vol. 81, no. 1, pp. 16–21, 2012.

[91] E. Martinho, "Calculation of total absorbed doses in research reactors," *Kerntechnik*, vol. 61, no. 2–3, pp. 122–127, 1996.

[92] W. Bonzer, "Progress Report 2012 - 2013, Missouri University of Science and Technology Reactor."

[93] Z. a. Kulage, C. H. Castano, S. Usman, and G. Mueller, "Characterization of the neutron flux energy spectrum at the Missouri University of Science and Technology Research Reactor (MSTR)," *Nucl. Eng. Des.*, vol. 261, pp. 174–180, 2013.

[94] R. S. Caswell, J. J. Coyne, and M. L. Randolph, "Kerma Factors of Elements and Compounds," *Int. J. Appl. Radiat. Isot.*, vol. 33, no. 11, pp. 1227–1262, 1982.

[95] "National Institute of Standard and Technology (NIST)." [Online]. Available: http://www.nist.gov/pml/data/index.cfm.

[96] "A General Monte Carlo N-Particle (MCNP) Transport Code, Los Alamos National Laboratory." [Online]. Available: https://mcnp.lanl.gov/.

[97]   B. Richardson, C. H. Castano, J. King, A. Alajo, and S. Usman, "Modeling and validation of approach to criticality and axial flux profile experiments at the Missouri S&T Reactor (MSTR)," *Nucl. Eng. Des.*, vol. 245, pp. 55–61, 2012.

[98]   R. Brewer, "Criticality Calculations with MCNP: A Primer," 2009.

[99]   C. C. Lin, *Radiochemistry in Nuclear Power Reactors*. 1996.

VITA

Maria Camila Garcia Toro was born in Medellin, Colombia. She was accepted into the Engineering School at the National University of Colombia in 2007 and graduated in April 2014 with a Bachelors of Chemical Engineering. During her undergraduate program, Maria Camila was a member of the research group in Electrochemical Engineering where she developed her thesis entitled "Construction and Characterization of anodes NiO-CGO for Hydrogen Oxidation in Intermediate-Temperature Solid Oxide Fuel Cells." During the summer 2013, she did an internship in the Department of Chemical and Biomolecular Engineering of the University of Tennessee, Knoxville, Tennessee, with the support of Dr. Thomas A. Zawodzinski and Dr. Gabriel Goenaga. She acted as a Graduate Research Assistant for the Nuclear Engineering Department of the Missouri University of Science and Technology. Her research was focused on the synthesis and characterization of radioactive nanostructures by neutron radiation and ionizing radiation in the Missouri University of Science and Technology research nuclear reactor (MSTR) to be used in cancer treatment, specifically on the synthesis of radioactive gold nanoparticles and bimetallic Au/ Ag nanoparticles. Maria Camila received her Master's degree in Nuclear Engineering in July 2016 from the Missouri University of Science and Technology, Rolla, Missouri, USA. Maria Camila was an active peer learning assistant in the Learning Enhancement Across Disciplines (LEAD) program in the Missouri University of Science and Technology. She was in charge of Nuclear Technology, Applications and Nuclear Materials and Spanish I (FS15) and Reactor Heat Transfer and Spanish I (SP16). Maria Camila was a student member of the American Nuclear Society (ANS) since 2016.